

AEDC-TR-88-22

C#4



Design and Operation of a Free Molecule Heat Transfer Probe

Frank G. Collins
The University of Tennessee Space Institute
Tullahoma, Tennessee 37388

December 1988

Final Report for Period February 1984 – December 1987

Approved for public release; distribution is unlimited.

**TECHNICAL REPORTS
FILE COPY**

PROPERTY OF U.S. AIR FORCE
AEDC TECHNICAL LIBRARY

**ARNOLD ENGINEERING DEVELOPMENT CENTER
ARNOLD AIR FORCE BASE, TENNESSEE
AIR FORCE SYSTEMS COMMAND
UNITED STATES AIR FORCE**

NOTICES

When U. S. Government drawings, specifications, or other data are used for any purpose other than a definitely related Government procurement operation, the Government thereby incurs no responsibility nor any obligation whatsoever, and the fact that the Government may have formulated, furnished, or in any way supplied the said drawings, specifications, or other data, is not to be regarded by implication or otherwise, or in any manner licensing the holder or any other person or corporation, or conveying any rights or permission to manufacture, use, or sell any patented invention that may in any way be related thereto.

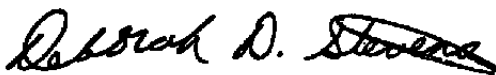
Qualified users may obtain copies of this report from the Defense Technical Information Center.

References to named commercial products in this report are not to be considered in any sense as an endorsement of the product by the United States Air Force or the Government.

This report has been reviewed by the Office of Public Affairs (PA) and is releasable to the National Technical Information Service (NTIS). At NTIS, it will be available to the general public, including foreign nations.

APPROVAL STATEMENT

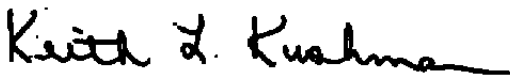
This report has been reviewed and approved.



DEBORAH D. STEVENS, 1st Lt, USAF
Directorate of Technology
Deputy for Operations

Approved for publication:

FOR THE COMMANDER



KEITH L. KUSHMAN
Technical Director
Directorate of Technology
Deputy for Operations

UNCLASSIFIED

SECURITY CLASSIFICATION OF THIS PAGE

REPORT DOCUMENTATION PAGE				Form Approved OMB No. 0704-0188	
1a. REPORT SECURITY CLASSIFICATION Unclassified			1b. RESTRICTIVE MARKINGS		
2a. SECURITY CLASSIFICATION AUTHORITY			3. DISTRIBUTION / AVAILABILITY OF REPORT Approved for public release; distribution is unlimited.		
2b. DECLASSIFICATION / DOWNGRADING SCHEDULE					
4. PERFORMING ORGANIZATION REPORT NUMBER(S) AEDC-TR-88-22			5. MONITORING ORGANIZATION REPORT NUMBER(S)		
6a. NAME OF PERFORMING ORGANIZATION University of Tennessee Space Institute		6b. OFFICE SYMBOL (if applicable)	7a. NAME OF MONITORING ORGANIZATION		
6c. ADDRESS (City, State, and ZIP Code) Tullahoma, TN 37388			7b. ADDRESS (City, State, and ZIP Code)		
8a. NAME OF FUNDING / SPONSORING ORGANIZATION Arnold Engineering Development Center		8b. OFFICE SYMBOL (if applicable) DOT	9. PROCUREMENT INSTRUMENT IDENTIFICATION NUMBER F40600-84-K0002		
8c. ADDRESS (City, State, and ZIP Code) Air Force Systems Command Arnold Air Force Base, TN 37389-5000			10. SOURCE OF FUNDING NUMBERS		
			PROGRAM ELEMENT NO	PROJECT NO	TASK NO
					WORK UNIT ACCESSION NO.
11. TITLE (Include Security Classification) Design and Operation of a Free Molecule Heat Transfer Probe					
12. PERSONAL AUTHOR(S) Collins, Frank G., University of Tennessee Space Institute, Tullahoma, TN					
13a. TYPE OF REPORT Final		13b. TIME COVERED FROM 2/84 TO 12/87		14. DATE OF REPORT (Year, Month, Day) December 1988	15. PAGE COUNT 88
16. SUPPLEMENTARY NOTATION Available in Defense Technical Information Center (DTIC).					
17. COSATI CODES			18. SUBJECT TERMS (Continue on reverse if necessary and identify by block number)		
FIELD	GROUP	SUB-GROUP	heat transfer free-molecule flow hot wire probe flow properties		
20	13				
19. ABSTRACT (Continue on reverse if necessary and identify by block number) This report describes the development of a free-molecule hot wire probe of unique design. When the probe is coupled with an independent measurement of number density or pitot pressure, it is capable of determining all of the flow properties at a point in a rarefied flow field. It has good spatial resolution and large dynamic range, and it is capable of obtaining measurements at densities below which some techniques, such as the electron beam, cannot be used. It can also be used to measure flow fields within nozzles which are not accessible to optical and electron beam techniques. Preliminary tests of the probe indicate its usefulness and convenience for making flow field measurements. Normalized measurements compared very favorably with those made with the pitot probe and electron beam. Continued development will be required before the probe can display its maximum utility.					
20. DISTRIBUTION / AVAILABILITY OF ABSTRACT <input type="checkbox"/> UNCLASSIFIED/UNLIMITED <input checked="" type="checkbox"/> SAME AS RPT <input type="checkbox"/> DTIC USERS			21. ABSTRACT SECURITY CLASSIFICATION Unclassified		
22a. NAME OF RESPONSIBLE INDIVIDUAL Mr. Carlton L. Garner			22b. TELEPHONE (Include Area Code) (615) 454-7813	22c. OFFICE SYMBOL DOCS	

DD Form 1473, JUN 86

Previous editions are obsolete.

SECURITY CLASSIFICATION OF THIS PAGE

UNCLASSIFIED

PREFACE

The work reported herein was conducted by the University of Tennessee Space Institute (UTSI), Tullahoma, TN, at the request of the Directorate of Technology, Arnold Engineering Development Center (AEDC), Arnold Air Force Base, Tennessee, under contract number F40600-84-K0002. The Air Force Project Manager was Mr Marshall Kingery; the UTSI Project Manager was Dr Frank G Collins. The reproductions used in the reproduction of this report were supplied by the author.

CONTENTS

	<u>Page</u>
1.0 INTRODUCTION	7
2.0 FREE-MOLECULE HEAT TRANSFER PROBE DEVELOPMENT	9
3.0 THEORY	11
3.1 Free-Molecule Heat Transfer to a Cross Stream Circular Cylinder . .	11
3.2 Heat Transfer Analysis of Probe	15
4.0 PROBE DESCRIPTION	20
4.1 Probe Construction and Calibration	20
4.2 Electronics	25
4.2.1 Description of Electronics and Operational Procedures . . .	25
4.2.2 Transfer Function and Accuracy of the Electronics	26
4.3 Probe Operation	28
5.0 MEASUREMENT RESULTS	30
6.0 CONCLUDING REMARKS	34
REFERENCES	35

ILLUSTRATIONS

Figure

1 C_F Versus ϵ for Lossless Nozzle in Vacuum, with γ as a Parameter. From Ref. 1	37
2. Nozzle Test Conditions	38
3. Modified Stanton Number for a Cylinder Transverse to the Flow Direction in Free Molecular Flow	39
4. Modified Recovery Factor for a Cylinder Transverse to the Flow Direction in Free Molecular Flow	40
5. Functions $f(s)$ and $g(s)$ Which Appear in the Expressions for the Free-molecule Heat Transfer to a Circular Cylinder	41
6. T_{aw}/T Versus Speed Ratio for a Circular Cylinder in Free-molecule Flow	42

<u>Figure</u>	<u>Page</u>
7. Function Used by Muthoo and Brundin (Ref. 13) to Determine Speed Ratio	43
8. Function Used by Gottesdiener (Ref. 2) to Determine Speed Ratio . . .	44
9. Relationship Used by Gottesdiener (Ref. 2) to Determine Velocity . . .	45
10. Comparison of Convection (Q_c) and Radiation (Q_r) Heat Transfer Rates for the Following Conditions:	
$T_0 = 500^\circ\text{K}$, $T_w = 625^\circ\text{K}$, $\gamma = 1.4$, $\epsilon_w = 0.1$, $\alpha = 0.9$, $s = 3.0$	46
11. Q_r/Q_c for Fixed $nV = 8 \times 10^{23}/m^2s$. $T_0 = 500^\circ\text{K}$, $\gamma = 1.4$, $\epsilon_w = 0.1$, $\alpha = 0.9$, $s = 3.0$	47
12. Construction of Hot Wire Probe	48
13. Detail of Connections at End of Wire	49
14. Microphotographs of Free-molecule Hot Wire Probes	50
15. Spot Welder Used to Attach Wire to Support Posts	51
16. Resistance-temperature Characteristic of Glass-coated Thermistors Manufactured by Victory Engineering Corporation	52
17. Probe Calibration Equipment	53
18. Measured Resistance of 1/8 Inch Probe	54
19. Measured Resistance of Thermistors on 1/8 Inch Probe	55
20. Measured Resistance of 1/4 Inch Probe	56
21. Measured Resistance of Thermistors on 1/4 Inch Probe	57
22. Probe Radiation Shield	58
23. Total Emittance of Platinum 13% Rhodium Alloy. (From Ref. 16)	59
24. Hot Wire Control	60
25. Bridge Decade Resistor	61
26. Proportional Temperature Control	62
27. Photograph of Free-molecule Heat Transfer Probe Electronics	63
28. Photograph of Hot Wire Control Module	64
29. Photograph of Proportional Temperature Controller Module	65
30. Bridge Calibration	66
31. Bridge Calibration	67
32. Probe Measurements for Run Number 26. Probe Located Outside plume Shear Layer. Overheat Ratio 1.19	68
33. Probe Measurements for Run Number 38. Probe Located Inside Nozzle. Overheat Ratio 1.025	69
34. Radial Profiles of Heat Transfer Coefficient Measured by Hot Wire Probe	70
35. Radial Profiles of Adiabatic Wall Temperature Measured by Hot Wire Probe	71

TABLES

	Page
1. Operating Parameters of Hot Wire	72
2. Hot Wire Measurements From Nozzle Tests	73

APPENDIXES

A. Free-Molecule Flow Properties Downstream of a Rectangular Orifice	75
NOMENCLATURE	83

1.0 INTRODUCTION

The space transportation systems of the future will require new and unique propulsion systems. This will especially be true for the engines that will be on orbit transfer vehicles, which will remain semi-permanently in space. The rocket motors on such vehicles will likely have very high chamber pressures, high values of I_{sp} , will be throttleable and will have the ability to start or stop frequently.

The orbit transfer vehicle engines will also be required to have a nozzle with a very large area ratio to maximize the thrust for given chamber pressure. The thrust can be conveniently written in terms of C_{F_x} , the thrust coefficient, by the following relation

$$T = C_{F_x} p_c A_t$$

where p_c is the chamber pressure and A_t is the nozzle throat area. The thrust coefficient is a maximum when the nozzle exit pressure is equal to the pressure of the surrounding atmosphere and when the nozzle is lossless. For lossless operation, $C_F = C_{F_x}$, where C_F is the thrust coefficient for isentropic nozzle flow. When the external pressure is essentially zero, which would be the case for an orbit transfer vehicle, then C_F reaches an asymptotic limit when the area ratio, $\epsilon = A_e/A_t$, becomes very large (A_e is the nozzle exit area). C_F is seen to increase by 8% as ϵ is increased from 50 to 1000 for $\gamma = 1.2$, for example (Fig. 1). Thus, there are advantages for increasing the area ratio if the losses can be demonstrated to be low.

High expansion ratio nozzles will create unique design problems which have not previously been encountered. The flow in the nozzle will not be isentropic, especially in the boundary layers on the wall. The boundary layer will be turbulent at the nozzle entrance but can be seen to undergo a dramatic change in properties before it reaches the nozzle exit, even if one ignores the effects upon it of chemical reactions and chemical and vibrational relaxation. During the nozzle expansion the boundary layer will undergo reverse transition and become laminar. By the time it has reached the exit the flow will have expanded to such an extent that rarefaction effects will be noticeable within the boundary layer. This set of flow circumstances will present a challenge to the rocket motor designer who will have to make a very accurate estimate of the thrust coefficient reduction to be expected for any particular nozzle design.

Because the physics of such boundary layer flows are so poorly understood it will be important to validate design codes for large expansion ratio nozzles by testing prototype nozzles before any such nozzles are constructed. Most conventional flow measurement tools will be incapable of examining the boundary layer near the nozzle exit because the local density will be too low. Non-intrusive sensing techniques (Raman scattering, laser fluorescence, etc) will not be usable inside the structure. Therefore, new techniques of observation will be required.

This report describes the preliminary development of a device which can be used to measure rarefied flow fields, such as the boundary layer near a nozzle exit.

The device is a hot-wire heat transfer probe which operates in free-molecule flow; it is a modification of the hot-wire probe developed by Gottesdiener (Ref. 2). The probe can be used to measure the flow properties within the boundary layer of a large expansion ratio nozzle or other nozzle when the local flow density is relatively low. Since the wire diameter is 10^{-4} inches, the present probe can operate in any flow where the local mean free path is greater than 5×10^{-4} inches. It could also prove useful for measuring the flow within the rocket nozzle plume and in the backflow region, upstream of the nozzle lip. The latter region is of great interest for spacecraft contamination studies.

Although non-intrusive techniques are normally used to measure the plume and backflow regions, the hot-wire probe has some advantages over the use of these other methods. The hot-wire probes are relatively inexpensive and arrays of fixed or movable probes could be used in these regions. Normally the alignment problems are so severe for the non-intrusive techniques that the nozzle is moved rather than the measurement system. This technique could not be used for measuring the flow fields from very large nozzles. However, the hot-wire probe can be easily translated, both inside the nozzle and outside. In addition, the probe can resolve the very high gradients that exist at the nozzle lip (Refs. 3 and 4) better than the non-intrusive methods and can perform backflow measurements at lower densities than methods such as the electron beam.

A hot-wire probe measures flow properties by measuring the change in resistance of a heated filament which results from the convective cooling caused by the flow over the filament. In free-molecule flow the probe can be used to measure the adiabatic wall temperature and the convective heat transfer coefficient of the filament wall. Theoretical expressions for free-molecule flow can then be used to relate the Stanton number and recovery factor (non-dimensional forms of the convective heat transfer coefficient and adiabatic wall temperature) to the speed ratio (non-dimensional velocity). The adiabatic wall temperature quickly approaches its hypersonic limit and cannot be used to determine the speed ratio. The convective heat transfer coefficient approaches its hypersonic limit more slowly but depends upon parameters in addition to the speed ratio. However, the speed ratio can be accurately determined when the hot-wire probe measurement is coupled with an independent measurement of the impact pressure or number density. Once the speed ratio has been determined then the static temperature, pressure, density, velocity and enthalpy can be calculated. No calibration of the probe is required when it is used in free-molecule flow. However, the probe surface area, the temperature coefficient of resistivity of the wire material and the thermal accommodation coefficient of the wire surface in the flow must be known. In addition, effective values of γ and \tilde{R} for the flow must be known to calculate the flow properties.

The hot wire must be attached to support posts which are considerably larger than the wire. The conductive loss to the supports is much greater than the free-molecule convective heat transfer between the heated wire and the flow. Very special

design techniques were used to attempt to eliminate these support conduction losses.

The probe was used to make measurements of the flow field at the exit of a small low density nozzle. The nozzle configuration and nominal test conditions are shown in Fig. 2. Probe measurements were made inside the nozzle, at several locations downstream of the nozzle exit, and in the backflow region, upstream of the nozzle lip. Measurements of the heat transfer coefficient, normalized by the centerline value, compared very favorably with normalized impact pressure measurements and electron beam number density measurements.

A probe of this design had been previously used to measure a flow that was at ambient temperature (roughly 300°K). By contrast, great temperature extremes existed in the flow facility in which the present probe was used. The gas stagnation temperature was 500°K while the free-molecule recovery temperature was about 580°K, which required heating the probe wire to a maximum of 625°K. On the other hand, the nozzle walls were less than 500°K and the entire nozzle and flow were surrounded by a 77°K cryogenic pumping shroud. Under these conditions the radiation loss from the probe surfaces became much greater than the wire support conduction loss. Attempts were made to reduce this error but they were not entirely successful. Suggestions for further reducing the radiation error are given at the end of the report.

The probe used for the tests reported upon in this report had $L/D = 2280$ and was in free-molecule flow ($K_n > 5$) if $n < 8 \times 10^{16}/cm^3$. For the flow field into which it was inserted the Knudsen number based on the wire diameter was always greater than 80. Under these conditions the probe was essentially non-intrusive to the flow field.

The background for the development of the free-molecule heat transfer probe is described in Section 2.0. The theoretical description of the operation is given in Section 3.0 while the probe and accompanying electronics are described in Section 4.0. The measurement results are discussed in Section 5.0. Finally, suggestions for future improvements in the probe are given in Section 6.0.

2.0 FREE MOLECULE HEAT TRANSFER PROBE DEVELOPMENT

The probe that was designed was a modification of designs that have been successfully used by other investigators and ideas from various previous investigators were incorporated into the probe. The evolutionary development of the probe will be described in this section and mention will be made of the improvements that were made over previous probes. The present probe was used in a more severe environment (higher T_o , lower T_∞) than experienced by previous works, as explained in the Introduction.

The cross-stream cylinder was one of the first shapes to be examined theoretically in free-molecule flow (Ref. 5) and then the theory was applied to obtain

flow-field properties from the heat transfer measurements of a heated cross-stream cylinder. Sherman (Ref. 6) measured T_{aw} for a very long unheated wire that was passed through a low density plane shock wave and used this measurement to obtain the shock wave profile and thickness. Wong (Ref. 7) developed a more traditional hot wire that was used to make measurements of h_c and T_{aw} in rarefied flows at $M = 4$ and 6. Coupled with an assumption of isentropic flow he was able to use the measurements to obtain the Mach number (speed ratio) and stagnation temperature. Theoretical expressions were used to make corrections for conduction losses to the supports and radiation losses were found to be unimportant [$T_{aw} \sim 345^\circ\text{K}$, $T_w - T_\infty < 100^\circ\text{K}$]. Laurmann and Ipsen (Ref. 8) used this hot wire probe to make low density flow field measurements around two simple two-dimensional shapes at $M = 4$ and 6. They use an 8 inch long wire to get a very large length-to-diameter ratio to minimize the conduction error and found that large overheat ratios were required to accurately measure h_c and T_{aw} .

The heat conduction down the support prongs was the major problem with the free-molecule heat transfer probe described above and prevented its adoption as a standard low density measurement tool. In addition to this problem, Brown and Thomas (Ref. 9) pointed out that more heat was conducted through the supports when the probe was in a gas than when it was in a vacuum (while keeping the average probe temperature the same). Therefore, the conduction had to be addressed before the probe could be successfully used for flow measurements. While ignoring radiation, Rajasooria and Brundin (Ref. 10) developed a technique for directly determining the conduction losses by calibrating the probe in a free stream and in a vacuum. Their procedure also eliminated the need for directly determining the probe dimensions or average material thermal conductivity. Lord (Ref. 11) greatly extended the technique for determining the conduction end loss correction, again ignoring radiation, and extended the techniques to apply to fluctuation measurements in supersonic continuum flows (Ref. 12). Muthoo and Brundin (Ref. 13) used Lord's correction technique and coupled the hot-wire measurements with those of the impact probe to obtain measurements of the speed ratio, pressure, temperature, stagnation temperature, density, velocity and enthalpy behind a sphere at a Mach number of 5.6. They resistively heated the support posts to minimize the conduction loss.

A major advance was made by Gottesdiener (Ref. 2) who placed small bead thermistors at the ends of the heated wire and used the thermistors as nonlinear heat sources in a temperature control system that essentially allowed the entire length of wire to be at a constant temperature. This directly eliminated the conduction loss and allowed the radiation corrections, which were applied to each measurement, to be measured under vacuum conditions. He used the probe in a free-jet flow where $M = 2$ and $p = 2 \times 10^{-5}$ torr. Coupled with electron beam density measurements, he was able to determine the flow speed ratio at the probe location. His design

has been basically copied for the probe that is described in Section 4.0. However, radiation presented a much greater problem than was confronted by any previous investigators and the probe was radiation shielded for measurements in the lowest density flows, especially when making measurements outside the nozzle where $T_\infty = 77^\circ\text{K}$.

3.0 THEORY

3.1 Free-Molecule Heat Transfer To a Cross Stream Circular Cylinder

The free-molecule flow over an infinitely long circular cylinder at right angles to the flow field can be determined by assuming that the cylinder wall temperature is constant over the entire surface, that the thermal accommodation coefficient is constant over the surface and that each molecule carries $j/2$ kT units of internal energy, where

$$j = \frac{5 - 3\gamma}{\gamma - 1}.$$

The thermal accommodation coefficient, α , is usually assumed to be the same for all modes of energy transfer since experimental evidence is lacking about the accommodation for internal energy. The flow is assumed to be uniform and in Maxwellian equilibrium. Then, the Stanton number and recovery factor are given by (Ref. 14) (see figures 3 and 4).

$$r = \frac{\gamma}{\gamma + 1} \frac{(3 + 2s^2)I_0\left(\frac{s^2}{2}\right) + (1 + 2s^2)I_1\left(\frac{s^2}{2}\right)}{(1 + s^2)I_0\left(\frac{s^2}{2}\right) + s^2 I_1\left(\frac{s^2}{2}\right)} \quad (1)$$

$$St = \frac{\alpha(\gamma + 1)}{4\gamma\sqrt{\pi}s} e^{-s^2/2} \left[(1 + s^2)I_0\left(\frac{s^2}{2}\right) + s^2 I_1\left(\frac{s^2}{2}\right) \right] \quad (2)$$

These expressions can be simplified by defining the following functions (Ref. 15)

$$Z_1 = \pi e^{-s^2/2} I_0\left(\frac{s^2}{2}\right) \quad (3)$$

$$Z_2 = \pi s^2 e^{-s^2/2} \left[I_0\left(\frac{s^2}{2}\right) + I_1\left(\frac{s^2}{2}\right) \right] \quad (4)$$

or the functions

$$f(s) = Z_1(s^2 + 3) + Z_2(s^2 + 7/2) \quad (5)$$

$$g(s) = 3(Z_1 + Z_2). \quad (6)$$

The functions f and g are plotted in Fig. 5. In terms of these functions

$$r = \frac{2\gamma}{\gamma+1} \frac{s^2 Z_1 + (s^2 + \frac{1}{2})Z_2}{s^2(Z_1 + Z_2)} = \frac{6\gamma}{\gamma+1} \frac{f(s) - g(s)}{s^2 g(s)} \quad (7)$$

$$St = \alpha \frac{\gamma+1}{\gamma} \frac{1}{4\pi^{3/2}s} (Z_1 + Z_2) = \alpha \frac{\gamma+1}{\gamma} \frac{1}{12\pi^{3/2}} \frac{g(s)}{s} \quad (8)$$

Also (see Fig. 6),

$$\frac{T_{aw}}{T} = \frac{f(s)}{g(s)} \quad (9)$$

Muthoo and Brundin (Ref. 13) combined these equations with the equation describing the measurement of an impact probe

$$p_i = pK(s) \quad (10)$$

to get the result

$$\frac{h_c \sqrt{2\pi T_{aw}}}{3p_i \sqrt{R}} = \alpha \left(\frac{\gamma+1}{\gamma-1} \right) \frac{\sqrt{f(s)g(s)}}{18\pi K(s)} \quad (11)$$

For $s > \sqrt{\gamma/2}$

$$K(s) = \left(\frac{\gamma+1}{\gamma} s^2 \right)^{\frac{\gamma}{\gamma-1}} \left[\frac{\gamma+1}{4s^2 - \gamma + 1} \right]^{\frac{1}{\gamma-1}} \quad (12)$$

Thus, measurements of h_c , T_{aw} and p_i yield the speed ratio, if α is known. The function in Eq. (11) is plotted in Fig. 7.

In contrast, Gottesdiener (Ref. 2) combined the hot-wire measurements with an independent measurement of the density, using the relation

$$F = 12\pi^{3/2} \frac{\gamma}{\gamma+1} \left\{ \frac{f(s)}{[g(s)]^3} \right\}^{1/2} = \alpha \sqrt{2R} c_p \frac{\rho \sqrt{T_{aw}}}{h_c} \quad (13)$$

to obtain the speed ratio. The velocity was then determined from a plot of

$$\frac{V}{\sqrt{2RT_{aw}}} = s \sqrt{\frac{g(s)}{f(s)}} \quad (14)$$

versus F . These relations are given in Figs. 8 and 9.

Once the speed ratio is known, plus either p_i or ρ , the remaining flow properties follow from Eqs. (9),(10), the definition of the speed ratio and assumptions of a perfect gas, namely,

$$p = \rho \tilde{R} T \quad (15)$$

and

$$H = \frac{\gamma}{\gamma - 1} \tilde{R}T \quad (16)$$

Certain asymptotic forms of Eqs. (1) and (2) are required for the data reduction or are useful for understanding the probe operation. First, consider the static gas approximation ($s = 0$). An expansion for the modified Bessel functions, valid near $s = 0$, is given by

$$\begin{aligned} I_\nu(z) &= \left(\frac{1}{2}z\right)^\nu \sum_{k=0}^{\infty} \frac{(1/4z^2)^k}{k! \Gamma(\nu + k + 1)} \\ I_\nu(z) &= \left(\frac{1}{2}z\right)^\nu \left\{ \frac{1}{\Gamma(\nu + 1)} + \frac{1/4z^2}{\Gamma(\nu + 2)} + \dots \right\} \\ I_0(z) &= 1 + \frac{1}{4}z^2 + \frac{1}{4} \left(\frac{1}{4}z^2\right) + \dots \\ I_1(z) &= \frac{1}{2}z + \frac{1}{16}z^3 + \dots \end{aligned} \quad (17)$$

Using the perfect gas expression for c_v , i.e.,

$$c_v = \frac{1}{\gamma - 1} \tilde{R}$$

and the definition of St , then, as $s \rightarrow 0$, we get to lowest order

$$h_c = \frac{\alpha \rho c_v V_m (\gamma + 1)}{4\sqrt{\pi}} = \frac{\alpha \rho c_v \tilde{c} (\gamma + 1)}{8} \left\{ 1 + \frac{1}{2}s^2 - s^4/16 \right\} \quad (18)$$

$$h_c = \alpha \left(\frac{\gamma + 1}{\gamma - 1} \right) \frac{p}{\sqrt{8\pi}} \sqrt{\frac{\tilde{R}}{T}} \quad (19)$$

The last form will be used to determine α from heat transfer measurements in a static gas.

$$r = \left(\frac{\gamma}{\gamma + 1} \right) \frac{(3 + 2s^2)I_0\left(\frac{s^2}{2}\right) + (1 + 2s^2)I_1\left(\frac{s^2}{2}\right)}{(1 + s^2)I_0\left(\frac{s^2}{2}\right) + s^2 I_1\left(\frac{s^2}{2}\right)}$$

Also,

$$r = \left(\frac{\gamma}{\gamma + 1} \right) \left(3 - \frac{15}{8}s^2 + \frac{7}{4}s^4 + \dots \right) \quad (20)$$

$$T_{aw} = T \left[1 + 3 \left(\frac{\gamma - 1}{\gamma + 1} \right) s^2 - \frac{15}{8} \left(\frac{\gamma - 1}{\gamma + 1} \right) s^4 + \dots \right] \quad (21)$$

The experiments were all performed at high values of s . In this case, $s \rightarrow \infty$ (Ref. 7)

$$Z_1 = \sqrt{\pi} \left(\frac{1}{s} + \frac{1}{4s^3} + \dots \right)$$

$$Z_2 = \sqrt{\pi} \left(2s - \frac{1}{2s} - \frac{3}{16s^3} + \dots \right)$$

and

$$St = \alpha \left(\frac{\gamma+1}{\gamma} \right) \frac{1}{2\pi} \left(1 + \frac{1}{4s^2} + \frac{1}{32s^4} + \dots \right) \quad (22)$$

Evaluating all properties at the static gas conditions approaching the probe and using the perfect gas expression for c_p , i.e.

$$c_p = \frac{\gamma}{\gamma-1} \tilde{R}$$

leads to

$$h_c = \alpha \frac{1}{2\pi} \left(\frac{\gamma+1}{\gamma-1} \right) nV k \left(1 + \frac{1}{4s^2} + \dots \right) \quad (23)$$

or

$$h_c = \alpha \frac{1}{\sqrt{2\pi}} \left(\frac{\gamma+1}{\gamma-1} \right) \rho \sqrt{T} \tilde{R}^{3/2} \left(s + \frac{1}{4s} + \dots \right) \quad (24)$$

Also,

$$g(s) = \sqrt{\pi} \left(6s + \frac{3}{2s} + \frac{3}{16s^3} + \frac{333}{128s^5} + \dots \right)$$

$$f(s) = \sqrt{\pi} \left(2s^3 + \frac{13}{2}s + \frac{21}{16s} + \frac{3}{32s^3} + \dots \right)$$

leading to

$$r = \frac{2\gamma}{\gamma+1} \left(1 - \frac{1}{8s^4} + \dots \right) \quad (25)$$

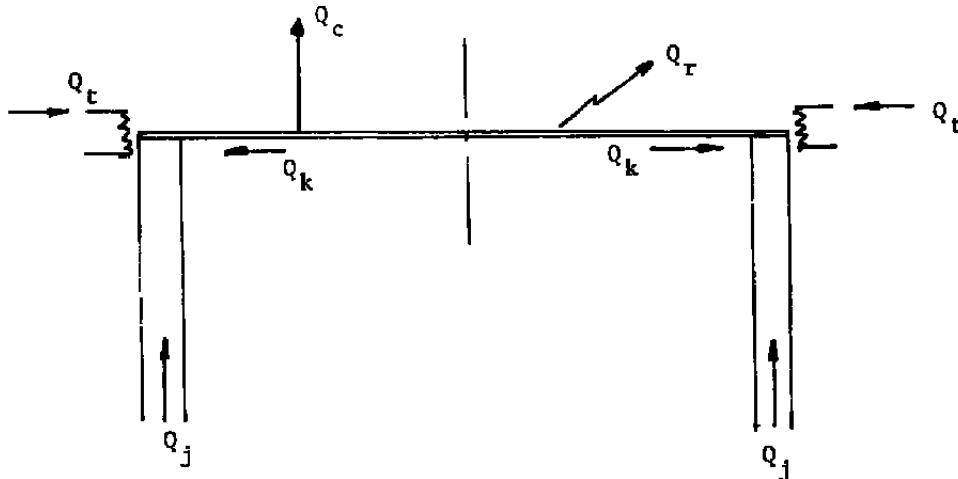
and

$$\frac{T_{aw}}{T_o} = \frac{2\gamma}{\gamma+1} \left[1 - \frac{1}{4s^4} + O\left(\frac{1}{s^6}\right) \right] \quad (26)$$

A comparison of Eqs. (23) and (26) indicates that T_{aw} approaches its asymptotic limit much faster than h_c does. Because the wall temperature is nearly constant for $s > 2$, the heat transfer coefficient must be measured at high speed ratios to obtain an accurate measurement of the local flow properties. However, a measurement of h_c alone will not result in the speed ratio. Therefore, either p_i must be measured and s determined from Eq. (11) or ρ must be measured and s determined from Eq. (13). External to the nozzle exit either could be measured, ρ by the electron beam technique, but inside the nozzle the impact pressure must be measured, along with the hot-wire probe measurements.

3.2 Heat Transfer Analysis of Probe

Consider the steady state heat transfer from a finite length wire mounted upon supports that are maintained at temperatures T_s by end heaters.



From an energy balance

$$Q_j + Q_t = Q_c + Q_r + Q_k . \quad (27)$$

It has been assumed that the supports are large compared to the wire so that there is negligible joulean heating of them. We can assume one-dimensional heat transfer in the thin cylindrical wire since $L/D \gg 1$. Introducing the heat transfer coefficient leads to the equation

$$h_c = \frac{Q_j + Q_t - Q_k - Q_r}{A_s(T_w - T_{aw})} \text{ (watts/m}^2\text{K)} . \quad (28)$$

Let the wire resistance be given by

$$R_w = R_a[1 + \alpha_r(T_w - T_a)]$$

where R_a is the resistance at the reference temperature T_a and α_r is the temperature coefficient of resistivity. Several reference temperatures have been tried and the only one that simplifies the analysis is

$$T_a = T_{aw}$$

where T_{aw} is constant at each probe location.

Thus,

$$R_w = R_{aw}[1 + \alpha_r(T_w - T_{aw})] . \quad (29)$$

Lord (Ref. 11) has examined the heat transfer to a hot wire probe and shown that it is possible to obtain experimental corrections for the heat losses due to conduction to the support posts. One of the useful features of his technique is that the effective wire length and diameter do not have to be measured but are determined by calibration. However, he ignored radiative heat transfer to the probe. The application to which the present probe was used does not allow for the neglect of radiation. Therefore, an attempt was made to extend the analysis of Lord to include radiative transfer. This analysis is included below, where it is assumed initially that $Q_i = 0$.

For a short length, dx , of the wire the energy balance equation can be written as (Refs. 7 and 11)

$$\begin{aligned} -\pi \frac{D^2}{4} \frac{d}{dx} \left[K_w \frac{dT_w}{dx} \right] + \pi Dh(T_w - T_{aw}) + \pi D \alpha \epsilon_w (T_w^4 - T_\infty^4) \\ = \frac{I^2 R_{aw}}{L} [1 + \alpha_r(T_w - T_{aw})] . \end{aligned} \quad (30)$$

It has been assumed that the wire is completely surrounded by a surface at a uniform temperature T_∞ and that all surfaces are gray.

A general solution to Eq. (30) cannot be written down without making some assumptions, because of the nonlinearity of the equation. It will be assumed that the wire thermal conductivity is constant along the wire and that the radiation term can be linearized. Because the probe will be operated with essentially uniform temperature over its length, the first approximation is valid. The linearization of the radiation term is not justified for the conditions under which the probe was used but must be done to get an analytical solution to the equation. However, in many cases it is justified. The method that was used for attempting to reduce the radiation term will be discussed in Sections 4.3 and 5.0.

Let $\theta = T_w - T_{aw}$, where θ will be assumed to be small compared to T_{aw} . Then,

$$T_w^4 - T_\infty^4 \simeq T_{aw}^4 \left\{ 1 + \frac{4\theta}{T_{aw}} - \left(\frac{T_\infty}{T_{aw}} \right)^4 \right\} . \quad (31)$$

Using this approximation Eq. 30 becomes

$$\frac{d^2 \theta}{dx^2} - A\theta = -B \quad (32)$$

$$A = \frac{4h_c}{DK_w} - \frac{4I^2\alpha_r R_{aw}}{\pi D^2 L K_w} + \frac{16\sigma\epsilon_w T_{aw}^3}{DK_w} \quad (33)$$

$$B = \frac{4I^2 R_{aw}}{\pi D^2 L K_w} - \frac{4\sigma\epsilon_w T_{aw}^4}{DK_w} \left[1 - \left(\frac{T_\infty}{T_{aw}} \right)^4 \right]. \quad (34)$$

This equation will be solved using the following boundary conditions

$$1. \quad T_w = T_s \text{ at } x = \pm L/2 \quad (35)$$

$$2. \quad \frac{dT_w}{dx} = 0 \text{ at } x = 0.$$

The solution is

$$T_w = T_{aw} + \left(T_s - T_{aw} - \frac{B}{A} \right) \frac{\cosh A^{1/2} x}{\cosh A^{1/2} L/2}. \quad (36)$$

This is the same solution given by Lord (Ref. 11) except that he ignored the radiation term.

The measured wire resistance is given by

$$R_w = \int_{-L/2}^{L/2} \frac{R_{aw}}{L} [1 + \alpha_r(T_w - T_{aw})] dx$$

$$R_w = R_{aw} + \frac{\alpha_r R_{aw} B}{A} + \left(R_s - R_{aw} - \frac{\alpha_r R_{aw} B}{A} \right) \frac{\tanh(A^{1/2} L/2)}{(A^{1/2} L/2)}. \quad (37)$$

For an infinitely long wire the resistance is given by

$$R_{w\infty} = R_{aw} + \frac{\alpha_r R_{aw} B}{A}. \quad (38)$$

Note that

$$A + \alpha_r B = C = \frac{4h_c}{DK_w} + \frac{16\sigma\epsilon_w T_{aw}^3}{DK_w} - \frac{4\alpha_r\sigma\epsilon_w T_{aw}^4}{DK_w} \left[1 - \left(\frac{T_\infty}{T_{aw}} \right)^4 \right]. \quad (39)$$

Then

$$R_{w\infty} = \frac{\alpha_r B}{C} R_{w\infty} + R_{aw}. \quad (40)$$

We can write

$$\frac{\alpha_r B}{C} = \left(\frac{4\alpha_r R_{aw}}{C\pi D^2 L K_w} \right) I^2 - \frac{4\alpha_r\sigma\epsilon_w T_{aw}}{CDK_w} \left[1 - \left(\frac{T_\infty}{T_{aw}} \right)^4 \right]$$

$$= XI^2 - Y; \quad (41)$$

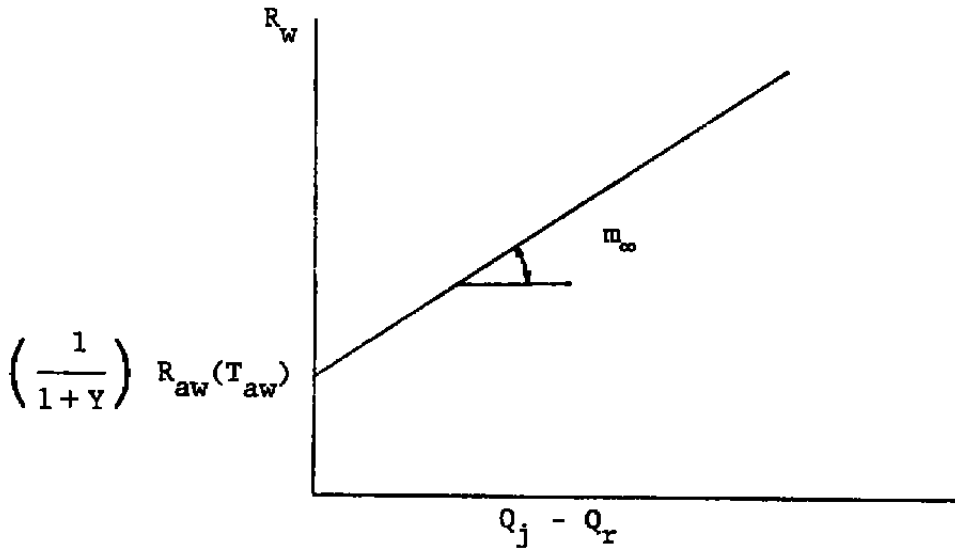
then

$$R_{w\infty} = \left(\frac{X}{1+Y} \right) (I^2 R_{w\infty}) + \left(\frac{1}{1+Y} \right) R_{aw} . \quad (42)$$

Thus, $R_{w\infty}$ versus $I^2 R_{w\infty}$ is a straight line with slope

$$m_{\infty} = \frac{X}{1+Y} \quad (43)$$

and intercept $\left(\frac{1}{1+Y} \right) R_{aw}$



where

$$m_{\infty} = \frac{\alpha_r R_{aw}}{\pi DL(h_c + 4\sigma\epsilon_w T_{aw}^3)} \quad (44)$$

$$\frac{1}{1+Y} = 1 - \frac{\alpha_r \sigma_w \epsilon_w T_{aw}^4 [1 - (T_{\infty}/T_{aw})^4]}{h_c + 4\sigma\epsilon_w T_{aw}^3} . \quad (45)$$

These are the expressions given by Lord (Ref. 11) with the addition of the radiation terms.

Thus, it is observed that the technique of Lord for correcting for the conduction to the supports cannot be used unless the radiation term can be neglected compared

to the convection. Consider a typical condition near the exit of the Mach number = 4 low density nozzle used during the measurements:

$$\text{gas} - \text{CO}_2, n = 10^{21}/\text{m}^3, T_{aw} = 583^\circ\text{K}, T_\infty = 77^\circ\text{K}, V = 815\text{m/s}.$$

Then,

$$\frac{h_c}{4\sigma\epsilon_w T_{aw}^3} = 2.26.$$

From Eq. (23), h_c diminishes as nV diminishes and the radiation correction becomes even greater as the probe is moved downstream into the nozzle plume.

This large magnitude of the radiation contribution invalidates the correction procedure of Lord (Ref. 11). In the present case, it was attempted to eliminate the conduction correction by placing thermistors, used as heaters, at the ends of the wire and applying power such that

$$Q_t = Q_k. \quad (46)$$

Assuming that this is possible Eq. (28) becomes

$$h_c = \frac{Q_j - Q_r}{A_s(T_w - T_{aw})} \text{ watts}/\text{m}^2\text{K}. \quad (47)$$

Radiation was a considerably greater problem for the probe when used for the present tests than for the tests of previous investigators because of the high stagnation temperature and correspondingly high adiabatic wall temperature (500°K and 583°K , respectively) and because the walls of the chamber were cooled with liquid nitrogen. A simple radiation heat transfer analysis of the probe would assume that the probe was surrounded by walls at a temperature T_∞ and that all walls were gray. The rate of radiative heat transfer would then be given by

$$Q_r = \epsilon_w A_s \sigma (T_w^4 - T_\infty^4) \quad (48)$$

where ϵ_w is the emissivity of the probe (less than 0.1 for the present probe).

One way to compare the influence of radiation on the probe is to compute the ratio of the radiation to convection heat transfer rates, Q_r/Q_c , given for large speed ratios by the ratio of Eq. (48) to (23), i.e.

$$\frac{Q_r}{Q_c} = \frac{\sigma\epsilon_w(T_w^4 - T_\infty^4)}{(\alpha A_s/2\pi) \left(\frac{\gamma+1}{\gamma-1}\right) nV k (1 + 1/4s^2)(T_w - T_{aw})}. \quad (49)$$

This ratio becomes large under the following circumstances: nV becomes small, T_w much greater than T_∞ , or T_w approaches T_{aw} .

First, consider the situation when the product nV becomes small. This case is shown in Fig. 10, for particular values of the other parameters. Radiation is less than convection to the right of the curve and becomes important at a higher value of nV as T_∞ decreases. At the centerline of the nozzle for the present tests (see Fig. 2) $nV = 4.8 \times 10^{24}/m^2s$. Thus, at that point $Q_c > Q_r$. However, at the nozzle lip the velocity was less and the number density less by a factor of at 5, than at the centerline, so that $Q_r > Q_c$. This also occurred in the backflow region, where the number density was considerably lower. The problem was more severe in the plume and backflow region where $T_\infty \simeq 77^\circ K$ for a considerable solid angle, whereas $T_\infty \simeq 470^\circ K$ within the nozzle. This problem is accentuated as T_w approaches T_{aw} (low overheat). Note that there must be an error in the paper by Gottesdiener (Ref. 2) who indicated that $Q_r = Q_c$ at $n = 4 \times 10^{17}/m^3$; the present analysis indicates that this occurs at much higher values of number density is also dependent upon the velocity.

For a given value of nV , Q_r/Q_c increases as T_w approaches T_{aw} , i.e., as the overheat ratio decreases. This effect, also noticed by Laurmann and Ipsen (Ref. 8), is illustrated in Fig. 11, which gives Q_r/Q_c as a function of T_w for given values of the other parameters. It will be shown in Section 4.3 that the probe must be operated at a number of overheat ratios and the R_w versus $(Q_j - Q_r)$ curve must be extrapolated to zero overheat. The radiation correction and, correspondingly the uncertainty in the measurement, will increase as the overheat ratio decreases.

The above analysis has considered the radiation only from the heated filament. However, potentially the major source of radiation loss is from the surface of the thermistors. The thermistors and thermocouples were attached to the support posts with a high temperature casting resin which created a black spherical blob at the end of the wire which had a diameter that was estimated to be less than 0.020 inches in diameter (see Fig. 14). The surface area of the resin spheres was up to 35 times larger than that of the wire and could correspondingly radiate a couple of orders of magnitude more power than the wire. Evidence that this could actually be the case is given in Section 5.0 and suggestions for significantly reducing this loss will be given in Section 6.0.

4.0 PROBE DESCRIPTION AND OPERATION

4.1 Probe Construction and Calibration

The probe construction is shown schematically in Figs. 12 and 13 and a prototype of the probe is photographed in Fig. 14. Two probes, having nominal wire

lengths of 1/8 and 1/4 inches, were constructed. The heated element consisted of a 100×10^{-6} inch diameter Pt-10% Rh wire. This wire was manufactured by the Wollaston process and had a silver sheath that was removed by a 50% nitric acid solution. The wire was attached to 0.003 inch diameter constantan posts which were in turn mounted to 0.020 inch diameter constantan supports. Normally the wires would be attached to nickel supports but constantan has one-fourth the thermal conductivity of nickel and its use minimized the conduction loss from the ends of the wire. The constantan posts were silver soldered to the .020 inch diameter constantan supports with a eutectic silver solder and the Pt-10% Rh wire was spot welded to the 0.003 inch diameter constantan posts using the spot welder shown in Fig. 15.

Following Gottesdiener (Ref. 2), thermistors were placed at the ends of the wire in an attempt to eliminate the conduction losses by heating the ends of the wire an amount so that $Q_t = Q_k$. Thermistors are useful heating elements to use in proportional temperature controllers because of their rapid variation of resistance with temperature. The thermistors used were VECO 0.013 inch diameter bead thermistors with a resistance of 1000 ohms and dissipation constant of $0.10mw/^\circ C$. They could deliver a maximum power of 0.012 watts. The temperature variation of the thermistor resistance is shown in Fig. 16. The end temperatures were sensed with 0.002 inch diameter chromel-alumel thermocouples. The thermocouple wires were insulated and enclosed in a 0.010 inch outside diameter stainless steel sheath. The thermocouples and thermistors were attached to the constantan posts with Stycast 2762 FT, which is a high temperature casting resin that possesses a high thermal conductivity. Before attaching the thermocouples and thermistors, the constantan posts were coated with Cal Custom #8028 white high temperature paint. The Pt-10% Rh wires were attached after the thermocouples and thermistors were in place.

The constantan supports were glued into a ceramic support that consisted of a cluster of multi-holed ceramic tubes. The ceramic tubes, in turn, were mounted inside a stainless steel tube. The thermocouple and thermistor lead wires were led through the remaining holes in the ceramic tubes. See Figs. 12 and 13 for construction details.

The stainless steel tube was supported on a traverse inside the vacuum chamber that allowed it to be rotated and translated with respect to the plane of symmetry of the nozzle. The short length of the wires allowed the probes to be positioned to within several thousandths of an inch of the nozzle wall. This was more than adequate to resolve the properties through the nozzle wall boundary layer and their diameter was small enough to resolve the high flow gradients in the nozzle lip region.

The probes were constructed and calibrated by personnel of Calspan Field

Services, Inc., AEDC Division, at Arnold Air Force Station. It is very crucial that the probe resistance and temperature coefficient of resistivity be known very accurately (to 0.1%) to accurately use the probe to measure flow properties. The equipment used to calibrate the probe is shown in Fig. 17. The probe and an RTD probe were placed in a large steel block which was placed in an oven. The oven temperature was increased to greater than 500°F and the oven power was turned off. The RTD probe was connected to a Fluke 2180A RTD digital thermometer, whose output was fed to the HP computer. Data were taken when the oven cooled to 500° and at approximately each 10°F decreased until the temperature reached 80°F.

The probe wire and each thermistor (TM1 and TM2) were attached to the voltage divider circuit shown in Fig. 17, where the value of the divider resistor is indicated. The two thermocouples (TC1 and TC2) were connected to a Kaye ice point reference. All voltages were measured with a Fluke 8502A voltmeter after passing through a Fluke 2204A scanner. The four wire technique was used to measure all the voltages. Input voltages of approximately 2,4,6,8, and 10 volts were applied to the voltage divider circuits. Thirty-two readings were internally averaged at each reading. The procedure at each oven temperature was as follows:

1. Read the oven temperature.
2. Read the voltage from TC1 and TC2.
3. Read the oven temperature.
4. Read the wire potential for the five values of E_i .
5. Read the oven temperature.
6. Read the TM1 potential for the five values of E_i .
7. Read the oven temperature.
8. Read the TM2 potential for the five values of E_i .
9. Read the oven temperature.

The calibration results are shown in Figs. 13 through 21. The probe wire resistances are shown in Figs. 18 and 20 for the 1/8-inch and 1/4-inch probes, respectively, and the thermal coefficient of resistivity was determined from a least square fit through the measured points. The two determined values of α_r agree closely. The measured thermistor resistances are shown in Figs. 19 and 21. The measured thermocouple outputs corresponded closely to the standard tabulated values.

At very low values of the product nV the radiation heat transfer from the heated wire is much larger than the convection. When the probe was used in these

circumstances it had been planned to surround it by a double cylindrical radiation shield shown in Fig. 22. The inner shield was to consist of two layers of copper wire (30 mesh, 37% open area) which would have been laid at 45° to one another. This shield would have contained an insulated nichrome wire which would have heated it to the wire temperature. If the shape factor of this shield, from the probe, had been 1.0, then heating the shield to T_w would have eliminated the radiation error. However, the probe would no longer have been in free-molecule flow. Therefore, the wire mesh was to have been used; the molecules which struck the mesh would have been scattered in many directions with little probability of returning to the wire, and those that proceeded through the mesh would have been pumped by the outer cylinder, which was to be cooled with liquid nitrogen (CO_2 is effectively pumped at 77°K). This shielded arrangement would have allowed the probe to have been used in regimes never reached by previous investigators but it was never constructed. Therefore, it is not known how effective it might have been in reducing the radiation loss. Instead, a simple shield consisting of a single helical coil of 0.3 inch diameter Nichrome wire was placed around the probe. A thermocouple that had been silver soldered to the Nichrome wire was used to measure the shield temperature and control the current through the wire. This shield was not very effective in reducing the radiation loss. Experience with this simple radiation shield will be discussed in Section 5.0.

Seban (Ref. 16) measured the emissivity of Pt-13% Rh for temperatures greater than 700°K (Fig. 23). He found that the emissivity greatly increased if the Rhodium oxidized (x data points). Care was taken to avoid wire oxidation during the manufacture and testing of the probe and the wire always seemed to maintain its shiny appearance. At the operating temperatures used in the experiments, the data in Fig. 23 indicates that $\epsilon_w < 0.1$. At any temperature the emissivity can be approximated by the equation

$$\epsilon_w = 0.576\sqrt{\rho_w T_w} - 0.179(\rho_w T_w) + 0.44(\rho_w T_w)^{3/2} \quad (51)$$

where ρ_w is the wire resistivity, in units of ohm cm, and T_w has the units of °K. The resistivity is given by

$$\rho_w = \rho_0 [1 + \alpha_r (T_w - 273)]. \quad (52)$$

For Pt-10% Rh, $\rho_0 = 18.4 \times 10^{-6}$ ohm, cm and $\alpha_r = 0.0017/^\circ\text{K}$. At $T_w = 625^\circ\text{K}$, this formula gives $\epsilon_w = 0.076$. A conservative value of 0.1 has been used in all the heat transfer calculations.

The heat transfer from the wire also depends on the thermal accommodation coefficient of the wire. The accommodation of both the translational and internal energies must be considered. Very little evidence exists about the accommodation

of internal energy but that which does exist indicates that the accommodation coefficients for CO₂ for translational and rotational energy are both equal to 1.0 while the accommodation coefficient for vibrational energy is small, so that the overall accommodation coefficient is 0.81 (Ref. 17). The possibility existed for nonequilibrium to occur in the exhaust of the nozzle, especially in the boundary layer and the lip and backflow regions. Since the lowest vibrational temperature of CO₂ is 961°K and the stagnation temperature is only 500°K, there will be very little excitation of any of the vibrational modes, especially at the nozzle exit where the temperature is about 120°K, and only rotational nonequilibrium needs to be considered. Assuming equal values of the translational and rotational accommodation coefficients, Sherman (Ref. 6) derived the free-molecule result

$$\frac{T_{aw}}{T_t} = \frac{f(s)}{g(s)} + \frac{1}{3} \left(\frac{T_r}{T_t} - 1 \right) \quad (53)$$

which gives the same result as Eq. (9) when the translational static temperature T_t , equals the rotational temperature, T_r . Using this result, he calculated the difference in T_{aw} downstream of a shock wave in a diatomic gas, assuming that T_r , remained at the upstream temperature, and compared it to the result that would be obtained for equilibrium flow. Even at an upstream Mach number of 4, the difference in wall temperature was only about 2%. Thus, even in such a severe nonequilibrium flow as a normal shock wave, the effect of rotational non-equilibrium on the wire temperature can be neglected as long as the accommodation coefficients for translational and rotational energy are equal.

A greater error than that caused by the nonequilibrium flow is caused by flow gradients along the wire length. Traditionally free-molecule wire probes have been long (up to 8 inches) to minimize the conduction loss. The present probes were considerably shorter and therefore could be used in regions of larger temperature gradients.

The following heat transfer rate formulas were used to assist in the design of the electronics and the experiments. They apply to the 1/4-inch wire for the conditions: gas - CO₂, $V = 815\text{m/s}$, $n = 5.85 \times 10^{21}/\text{m}^3$, $s = 3.25$, $\alpha = 0.9$, $\epsilon_w = 0.1$.

$$Q_c = 2.94 \times 10^{-6} [T_w - T_{aw}] \text{ watts} \quad (53)$$

$$Q_r = 2.88 \times 10^{-16} [T_w^4 - T_{\infty}^4] \text{ watts.} \quad (54)$$

An upper estimate of the radiation from the resin surrounding the two thermistors is given by the following formula.

$$Q_r (\text{thermistors}) \approx 9.1 \times 10^{-14} [T^4 - T_{\infty}^4] \text{ watts} \quad (55)$$

where T is the unknown surface temperature of the resin. This formula assumes that the diameter of the black resin is 0.020 inches and the emissivity of the surface is 1.0.

4.2 ELECTRONICS

4.2.1 Description of Electronics and Operational Procedures.

Two separate electronic circuits were required to operate the probe, the first to maintain the wire at a prescribed resistance and the second to maintain the ends of the wire at the temperature which corresponds to the prescribed wire resistance. The circuit schematics are given in Figs. 24 to 26 and photographs of the completed instruments are given in Figs. 27 through 29.

The wire was maintained at a constant mean temperature with an open loop constant-current anemometer circuit and was used much as a constant-current anemometer is used to measure flow temperature. The circuit was designed to meet the special needs of the present probes which included greatly increased probe resistance (100 to 300 ohms, compared to usual hot wire probe resistances of 5 to 10 ohms) and the need to operate at very small overheat ratios which require small amounts of power (to 10^{-6} watts). A 20:1 bridge was used to increase the sensitivity of the measurement and the probe was placed in one leg of that bridge (Fig. 24). Initially a closed loop system was designed but the bridge imbalance required to obtain stable feedback behavior prevented that technique from yielding accurate measurements of the probe resistance.

The hot wire control is operated in the following fashion.

1. Ground both inputs to the current source amplifier and balance the amplifier.
2. Place a calibration resistor in place of the hot wire [$100.04 \pm 0.01\Omega$ resistor for 1/8 inch probe; $200.55 \pm 0.1\Omega$ resistor for 1/4 inch probe] and set the thumbwheel resistor to the value to balance the bridge [200 and 401, respectively]. Offset the current amplifier by 0.100 volts and adjust the bridge imbalance measuring amplifier until its output is zero, as read by M4.
3. Replace the calibration resistor with the hot wire probe.
4. A desired probe resistance can be obtained by dialing the appropriate value on the thumbwheel resistor and changing the voltage offset to the current source until the bridge is balanced (meter reading M4 is zero).

The current limit is set by placing the meter at position M4, increasing the offset voltage on the current source until the maximum desired voltage is just exceeded, and then adjusting the potentiometer on the FET until the voltage just begins to decrease. Generally the bridge top voltage was adjusted to limit the probe current to about 0.6 *ma*, although the probes were able to handle 20 *ma* in air without being destroyed.

Because of the large conduction heat loss from the wire to the support posts, a large temperature gradient will exist in the wire until power is applied to the thermistors. The purpose of the proportional temperature controllers is to apply sufficient power to the thermistors to bring the wire ends to the temperature which corresponds to the mean wire resistance, as set by the wire control (see eq. (58)). This is accomplished by the following steps (see Fig. 26).

1. Balance the input to the two amplifiers. In switch positions M1 and M2 the input to the amplifiers are grounded and the outputs are open. Position M1 is used to balance the first stage and M2 the second stage of amplification.
2. Measure the output of the thermocouple transducer in switch position M4 with the loop still open and the amplifier inputs grounded. Set the offset to the first stage (10 turn potentiometer) to a voltage just slightly greater than the thermocouple transducer voltage.
3. Close the loop and set the desired temperature by adjusting the offset to give the desired temperature (see Eq. (62)).

The maximum power that the thermistors can dissipate is approximately 0.012 watts. The power is limited by attaching a resistor of appropriate size at the thermistor input (the resistor magnitude depends on the expected operating temperature), increasing the offset voltage on the first amplifier stage until the maximum possible voltage is achieved at the upper end of the resistor and then adjusting the potentiometer on the FET transistor until the voltage begins to drop.

4.2.2 Transfer Function and Accuracy of The Electronics.

If the resistors in the bridge were perfectly balanced then the bridge output as measured by the voltage across the bridge (M3) would be zero when the thumbwheel resistor was precisely 20 times the wire resistance. This could be determined by placing a small current through the bridge from the current source and measuring the voltage M3. However, no attempt was made to perfectly match the resistors and instead the transfer function of the bridge was measured. First, the bridge was balanced as outlined in steps 1 and 2 in the previous section. Then the calibration resistor was replaced with a variable resistor called Dekabox, manufactured by

Electro-Measurements, Inc. The resistance values from the Dekabox were measured with a Fluke 8040A multimeter and found to have an accuracy of 0.3 to 0.1 Ω , as the total resistance varied from 100 to 380 Ω , respectively. The offset voltage on the current source (E_2) was placed at 0.800, 1.200 and 1.600 volts and although small differences were seen as the offset voltage varied they were much smaller than the overall imbalance condition of the bridge and all measurements were averaged together.

The transfer function was determined by setting the Dekabox resistance value (range 100 to 200 Ω for the 1/8 inch probe and 200 to 380 Ω for the 1/4 inch probe) and determining the value of the thumbwheel resistor that balanced the bridge. The measurements are shown in Figs. 30 and 31 and indicate that a linear regression line through the measurements was adequate. The results are as follows:

A) 100.04 Ω calibration resistor

$$R_i \text{ (input)} = 1.38 + 0.96786R_m \text{ (measured on thumbwheel)} \quad (56)$$

Mean of deviation: 0.16 Ω

Standard deviation: 0.10 Ω

B) 200.55 Ω calibration resistor.

$$R_i \text{ (input)} = 4.21 + 0.95524R_m \text{ (measured on thumbwheel)} \quad (57)$$

Mean of deviation: 0.26 Ω

Standard deviation: 0.31 Ω

The resolution of the variable thumbwheel resistor is 0.5 Ω (10/20). Therefore, both regression lines are within the resolution of the instrument and the basic resistance measuring accuracy of the instrument is comparable to the instrument resolution. For those run conditions when E_2 was less than 0.800, the following equation was used to determine the input resistance.

$$R_i \text{ (input)} = C \times R_m \text{ (measured on thumbwheel)} \quad (58)$$

E_2 (volts)	C
0.200	0.9890
0.300	0.9845
0.400	0.9810
0.500	0.9790
0.600	0.9776
0.700	0.9768

The probe resistance is given by the equation

$$R_w = R_{20}[1 + \alpha_{20}(T_w - 293)] \quad (59)$$

where the reference state is taken to be 20°C. The uncertainty in temperature is related to the uncertainty in resistance by the relation

$$\Delta T = \frac{\Delta R}{\alpha_{20} R_{20}} \quad (60)$$

Using the conservative estimate $\Delta R = 0.5\Omega$ and the values of R_{20} and α_{20} obtained from the probe calibration (Figs. 18 and 20) then

$$\Delta T = \begin{cases} 2.6^\circ\text{K} & (1/8 \text{ inch probe}) \\ 1.5^\circ\text{K} & (1/4 \text{ inch probe}) \end{cases} .$$

Now consider the accuracy of the proportional temperature controllers. The basic Analogue Devices chip AD595CD has an accuracy of $\pm 1^\circ\text{K}$ and this will be the accuracy of the controllers if other uncertainties are not added to the system. First, the thermocouple outputs were measured for both thermocouples on each probe during the probe calibration and their outputs were found to agree closely with the standard tabulated values. Therefore, the tabulated thermocouple voltages were assumed to accurately represent the signal from the thermocouples on the probes and were used to determine the temperature, without correction.

The transfer function of the device AD595CD, as given by the manufacturer is,

$$E = 247.3[(mv) + 11 \times 10^{-6}] \text{ volts} \quad (61)$$

where E is the output voltage of the device for a Type K input voltage (mv). E was measured to $\pm 1mv$. This equation was solved for the (mv) input from the thermocouple and the standard tables were used to determine the temperature. The device accuracy of $\pm 1^\circ\text{C}$ represented the overall accuracy with which the temperature of the ends of the wire could be set, which at times was not accurate enough because of the low overheat values that were used, especially when there was a very small amount of convective cooling (see Section 5.0).

4.3 Probe Operation

The free-molecule heat transfer probe measures the convective heat transfer coefficient and the adiabatic wall temperature of the wire. As previously discussed, kinetic theory can yield theoretical expressions relating these quantities (i.e., h_c and T_{aw}) to the properties of the flowing fluid. A measurement of T_{aw} could be used to determine the speed ratio. However, as seen from Eq. (26) T_{aw} is very insensitive

to the speed ratio for large speed ratios and cannot be usefully used to determine the speed ratio. Likewise, the speed ratio cannot be directly determined from a measurement of h_c because the convective heat transfer coefficient depends upon flow properties in addition to the speed ratio, as seen in Eqs. (23) and (24). Therefore, to obtain an expression from which the speed ratio can be directly determined with accuracy at a high speed ratio, an independent measurement must be made of another quantity, either the impact pressure [Eq. (11)] or the density [Eq. (13)]. The procedures for obtaining the remaining flow properties once the speed ratio has been determined were outlined in Section 3.1.

The convective heat transfer coefficient and the adiabatic wall temperature of the probe are determined at each probe location as follows.

A desired wire temperature is obtained by setting the bridge to the resistance corresponding to the wire temperature, according to Eq. (59), namely

$$R_w = T_{20}[1 + \alpha_r(T_w - 293)]. \quad (59)$$

T_w should be greater than T_{aw} but the ratio T_w/T_{aw} had to be less than about 1.07 because the thermistors and glues could only operate to about 625°K. Next, power is applied to the thermistor heaters to bring the ends of the wire to the temperature T_w . This step was not possible for the experiments that were performed, as explained in Section 5.0. At this condition $Q_i = Q_k$ and Eq. (28) becomes

$$h_c = \frac{Q_j - Q_r}{A_s(T_w - T_{aw})}. \quad (62)$$

From the hot wire circuit diagram (Fig. 24),

$$Q_j = \left(\frac{E_2 - E_3}{2471} \right)^2 R_w \quad (63)$$

where R_w is determined from the regression Eqs. (56) or (57). Q_r can be determined by repeating the same measurement of Q_j under static conditions at a very low vacuum (10^{-5} torr or less). When the two measurements of Q_j are of comparable magnitude then the probe must be surrounded by the radiation shield and the experiments repeated. By replacing $(T_w - T_{aw})$ by Eq. (59) we find that

$$(R_w - R_{aw}) = \frac{R_{20}\alpha_{20}}{h_c A_s} (Q_j - Q_r) \quad (64)$$

and

$$\frac{dR_w}{d(Q_j - Q_r)} = \frac{R_{20}\alpha_{20}}{h_c A_s}. \quad (65)$$

Therefore, h_c is obtained from the slope and R_{aw} is given by the intercept of the curve of R_w versus $(Q_j - Q_R)$. T_{aw} is then determined from Eq. (59). At least five measurements must be made, at different values of R_w , both with and without flow (i.e., vacuum), to obtain an accurate measurement of the slope of the curve. This procedure must be repeated for each probe position. Once h_c and T_{aw} have been determined and either ρ or p_j has been measured at the same probe location, then the procedures outlined in Section 3.1 can be used to obtain the flow properties.

Before h_c or T_{aw} can be determined, the thermal accommodation coefficient of the wire must be known. It can be determined from static gas tests by using Eq. (19). h_c is determined as described above for various known values of p and T in a static vacuum chamber. For a 100μ inch wire, the chamber pressure must be below 1 torr for Eq. (19) to apply. Pressures in this range can be accurately measured with an MKS Baratron pressure transducer. Measurements at several values of p will yield an accurate measurement of the effective value of the accommodation coefficient of the probe wire. Unless the wire is used to measure flows that will contaminate the wire surface, α should not change with time. However, it would be helpful to occasionally repeat the measurement of α .

5.0 MEASUREMENT RESULTS

Preliminary use of the 1/4 inch free-molecule hot wire probe was made during the plume characterization tests in the 4' x 10' vacuum chamber at AEDC. Measurements were made in the plume of the nozzle (Fig. 2), in the backflow region, upstream of the lip, and inside the nozzle. The measurements were made without using the thermistors as heaters to eliminate the support conduction losses nor was the probe surrounded by a radiation shield. Pitot probe measurements were made simultaneously with the hot wire measurements. Comparison was made between these measurements and measurements of the number density, which had previously been obtained from electron beam measurements at the same locations. It was demonstrated that the hot wire measurements were able to resolve the structure of the flow field, although the magnitude of the measurements was in error. The opportunity did not exist during the duration of the tests to conclusively demonstrate the ability of the thermistor heaters and radiation shield to eliminate the conduction and radiation losses and additional experiments must be performed to examine their performance.

The probe was operated as described in Section 4.3. At each location the probe was operated at 5 or 6 overheat ratios. No attempt was made to measure the accommodation coefficient or the radiation loss, since the thermistor heaters were not used. The reason for not using the thermistors or a radiation shield will be discussed at the end of this section. Because α and Q_j were unknown, no attempt

was made to use the measured values of h_c and T_{aw} to determine the flow properties but rather normalized measurements were used to examine the flow structure. The measurements were also valuable because they provided an insight into the operation of the probe under severe temperature conditions.

The flow conditions can be summarized as follows: stagnation temperature 487° to 500°K, exit Mach number 4 and tunnel wall temperature (external to nozzle) 77°K. The probe operating range can be summarized as follows: heating power levels 4.9×10^{-6} to 1.432×10^{-4} watts, average wire temperature as determined from the average resistance, 324°K to 562°K, overheat range 1.025 (for measurements inside the nozzle) to 1.20 (for measurements in the backflow region), wire end temperatures measured by the thermocouples 303°K to 441°K, probe wire adiabatic wall temperature within the isentropic nozzle core flow 575.5°K, measured adiabatic wall temperature 308.5° to 543.7°K and measured wall heat transfer rate 12.4 to 170.0 watts/ m^2 °K. The probe calibration curve is shown in Fig. 20. The probe operating conditions and measurements of T_{aw} and h_c at each location are given in Tables I and II. Typical data analysis plots, from which these quantities were determined, are shown in Figs. 32 and 33. The low overheat ratios used for some tests indicate the importance of accurately knowing R_{20} and α_{20} for each wire.

The measurements indicate that large temperature gradients existed along the wire. These gradients resulted in large conduction and radiation losses. The extreme cases occurred for measurements that were performed within the nozzle, where the difference between the average wire temperature and the end thermocouple temperature was as high as 122°C (run number 40). At the other extreme were the measurements performed outside the plume and in the backflow region, where this temperature difference was 85°C (run number 28). Both of these temperature differences occurred at the maximum overheat ratio. Clearly, the heat losses are much too great to expect an accurate measurement of h_c and T_{aw} . Therefore, thermistor heating will be required to eliminate the conduction losses during future use of the probe.

Radiation heat transfer from the surface of the wire and the black resin surrounding the thermistors and thermocouples was also significant under the test conditions. This subject was discussed in Section 4.0. The radiation loss from the 1/4 inch wire could be accurately calculated from Eq. (53) if the wire was at a uniform temperature. However, since that was not the case, this formula could only give an estimate of the radiation loss by using the mean wire temperature as determined from the mean wire resistance. For a worst case estimate, T_∞ was assumed to be 77°K. This indicated that Q_r from the wire was in the range of 3.2×10^{-6} to 2.9×10^{-5} watts; these estimates are undoubtedly high.

Radiation heat transfer from the surface of the resin blobs, located at the ends

of the wire, was more difficult to estimate. The temperature internal to the resin was known from the thermocouple temperature but the surface temperature was unknown. Assuming that the resin blobs had a diameter of 0.020 inch, that their surface temperature was the same as the temperature indicated by the thermocouples and that the surface emissivity was 1.0, then the estimated radiation rate ranged from 7×10^{-4} to 3×10^{-3} watts. However, this is considerably greater than the power supplied to the probe, indicating that the surface temperature was much less than the indicated thermocouple temperature and/or the emissivity was much less than 1.0. Also, no consideration has been given in these estimates of the radiation shape factor between the walls at the various temperatures which existed within the 4' x 10' chamber. Nevertheless, the estimates indicate that radiation, as well as support conduction, produced a serious heat loss from the probe.

The measured profiles of h_c and T_{aw} in several radial planes are given in Figs. 34 and 35. Measurements were made at three downstream axial stations (5.74 inches, 3.74 inches and 0.74 inches, respectively). Some measurements were made inside the nozzle (-0.26 inches) and in the backflow region upstream of the lip (-0.26 inches). The hot wire probe was mounted adjacent to the pitot probe, as shown in Table II. The profile at 5.74 inches was taken across the entire plume profile but since it was symmetric the remaining profiles were taken only from the jet centerline (radial position 3.48 inches) outward. The measured values of h_c and T_{aw} were constant through the core of the plume and then fell rapidly in the shear layer. The measurements at location 0.74 inches indicate that the isentropic core was 3 inches in diameter at that location, which means that the shear layer was 0.5 inches thick. This is approximately the thickness of the boundary layer at the nozzle exit. The isentropic core then diminished and the shear layer greatly thickened as the flow expanded downstream. The actual flow adiabatic wall temperature was estimated to be roughly 578°K. This value was only approached as the measurement plane was moved upstream and inside the nozzle the measured value was 544°K. This lower value is the result of the conduction and radiation losses from the probe. In the backflow region at -0.26 inches (runs 28 and 29), h_c was measured to be 12.9 and 13.4 watts/m²°K, respectively. This was approximately the lower limit to the measurable heat transfer coefficient and resulted primarily from radiation rather than convection heat transfer. This conclusion is also confirmed by measurements made from a dummy probe that was placed in a vacuum ($p = 4 \times 10^{-3}$ torr) without any flow. The probe had not been calibrated so that its resistance, R_{20} , and surface area were not accurately known. Measured values of h_c with this probe in the vacuum were 11.88 and 11.45/watts/m²°K. These values are very close to the values measured in runs 28 and 29.

The opportunity did not exist during the tests to fully test the thermistor heaters on the radiation shield. Thermistor heating tests were performed on an early prototype probe which had a 1/4-inch long wire of diameter 2×10^{-4} inches.

This probe was uncalibrated and R_{20} was only approximately known (approximately 50 ohm). The tests demonstrated that the thermistor temperature controller could successfully control the thermistor power to place the thermocouple temperature at any desired set point. However, when power was applied to place the ends of the wire at the average wire temperature (as determined by the initial average wire resistance) the wire power, Q_j , was reduced to essentially zero at the bridge balance. In other words, the thermistors were heating the wire as well as the wire supports. Later analysis of these tests indicated that this was caused by an insufficiently accurate knowledge of R_{20} . The bridge electronics were designed for a probe having a resistance of $1000\ \Omega$ (1/4 inch long, 50×10^{-6} inch diameter wire). For such a wire the bridge balance resolution would be 0.05%. For the 200×10^{-6} inch wire, the bridge balance resolution was only 1%. Thus, both the lack of knowledge of R_{20} and the resolution of the bridge balance contributed to the uncertainty in the average wire temperature. In the tests under discussion it was estimated that the thermistors were heated to 7°C above the average wire temperature. This is not much greater than the expected accuracy of the bridge electronics (see Section 4.2.2). Therefore, the thermistor heaters will only be successful if the temperature can be measured with great accuracy, and if the resistance bridge has great resolution. This will require using a small diameter, calibrated probe if the present electronics are used.

The radiation shield shown in Fig. 22 was never constructed. However, a preliminary radiation shield test was performed on a damaged 1/8-inch probe. The probe was surrounded by a loosely-coiled Nichrome wire helix (0.03 inch diameter wire). The helix was about 5/8 inch in diameter and 2 1/4 inches long. The shield proceeded slightly forward of the wire. The probe was placed downstream of the exit of a low-density sonic orifice ($x/D \approx 30$, Mach number at probe ≈ 12 to 15). A chromel-alumel thermocouple was silver soldered to the Nichrome wire to determine the shield temperature.

The relevant parameters of the test are as follows. The gas was CO_2 with a stagnation temperature of 453° to 463°K . The shield could be heated only to 444°K with the DC power supply available. Without thermistor power the thermocouples on the wire posts measured 341°K . With maximum thermistor power (12×10^{-3} watts) this temperature was raised to 390°K , which is considerably below the stagnation temperature. However, without radiation shield heating or thermistor power the thermocouple temperature was reduced to 256°K . Therefore, the shield raised the thermocouple temperature 85°K even without thermistor power. This crude radiation shield had a noticeable influence on the temperature of the ends of the probe but was not sufficient to eliminate the radiation loss.

6.0 CONCLUDING REMARKS

The development of a free-molecule hot wire probe of unique design has been described in this report. When coupled with an independent measurement of number density or pitot pressure it is capable of determining all of the flow properties at a point in a rarefied flow field. It has good spatial resolution and large dynamic range, being capable of obtaining measurements at densities below which some techniques such as the electron beam cannot be used. It can also be used to measure flow fields within nozzles which are not accessible to optical and electron beam techniques.

The convective heat transfer coefficient, which is measured by the probe, is masked by influence of the conduction to the wire support posts. Thermistor heaters were placed at the ends of the wire to add sufficient energy to just compensate for this loss. The large surface area of the resin, which held the thermistors and accompanying thermocouples to the wire, created a large surface which could lose energy by radiation to the liquid nitrogen cooled surfaces which surrounded the flow field in the present tests. This loss must also be eliminated. That can be accomplished by using smaller thermistors (0.005 inch diameter as opposed to the 0.013 inch diameter thermistors used for the present tests) to reduce the radiating surface area and by using more efficient radiation shields. Future examination of the thermistors and radiation shield could more economically be performed in the free - molecule flow from a slit. The properties of this flow are well-known and are given in the Appendix for convenience.

Two electronic control circuits, one for controlling the wire temperature and the second for controlling the thermistor power, were designed and constructed. The tests indicate that the circuits performed very well, providing the accuracy and control required for the proposed use of the probe.

The preliminary tests that were performed with the probe indicated the usefulness and convenience of the probe for making flow field measurements. Normalized measurements compared very favorably with those made with the pitot probe and electron beam. Continued development will be required before the probe can display its maximum utility.

REFERENCES

1. Seifert, H. S., Editor, Space Technology, John Wiley and Sons, Inc., 1959, pp. 14-22.
2. Gottesdiener, L., "Hot Wire Anemometry in Rarefied Gas Flow," J. Phys. E. 13, 908-13 (1980).
3. Bird, G. A., "Breakdown of Continuum Flow in Freejets and Rocket Plumes," 12th Int. Symp. on Rarefied Gas Dynamics, Vol. 74, Prog. in Astron. and Aeron., AIAA pp. 682-694, (1980).
4. Bird, G. A., "The Nozzle Lip Problem," Proc. 9th Int. Symp. on Rarefied Gas Dynamics, DFVLR Press, Porz-Wahn, West Germany, Vol. I, ref. A. 22, 1974.
5. Stadler, J., G. Goodwin and M. O. Creger, "Heat Transfer to Bodies in a High-Speed Rarefied-Gas Stream," NACA Rept. 1093, 1952.
6. Sherman, F. S., "A Low-Density Wind-Tunnel Study of Shock-Wave Structure and Relaxation Phenomena in Gases," NACA TN 3298, July 1955.
7. Wong, H., "Design and Development of a Free-Molecule Heat-Transfer Probe," Univ. of Calif., Berkeley, Report No. HE-150-143, Oct. 15, 1956.
8. Laurmann, J. A. and I. C. Ipsen, "Use of a Free Molecule Probe in High Speed Rarefied Gas Flow Studies," WADC Tech. Rept. 57-440, Oct. 1957; J. A. Laurmann, "The Free Molecule Probe and Its Use for the Study of Leading Edge Flows," Phys. Fluids 1, 469-477 (1958).
9. Brown, R. E. and L. Thomas, "The Assignment of the Heat Flow From Electrically Powered Filaments to Gas Conduction for Accurate Measurement of Thermal Accommodation," 7th Int. Rarefied Gas Dynamics Symposium, Vol. I, Editrice Technico Scientifica, Pisa, Italy, pp. 347-355.
10. Rajasooria, G.P.D. and C. L. Brundin, "Use of Hot Wires in Low-Density Flows," AIAA J. 9, 979-81 (1971).

11. Lord, R. G., "Hot Wire Probe End-Loss Corrections in Low Density Flows," J. Phys. E. 7, 56-60 (1974).
12. Lord, R. G., "The Dynamic Behavior of Hot-Wire Anemometers with Conduction End Losses," J. Phys. E. 14, 573-578 (1981).
13. Muthoo, S. K. and C. L. Brundin, "Near Wake Flow Field Measurements Behind Spheres in Low Reynolds Number Hypersonic Flow," 9th Int. Sym. on Rarefied Gas Dynamics, DFVLR Press, Porz-Wahn, West Germany, ref. B. 10, 1974.
14. Schaaf, S. A. and L. Talbot, "Mechanics of Rarefied Gases," Handbook of Supersonic Aerodynamics, Sec. 16, NAVORD Report 1488 (Vol. 5), Feb. 1959.
15. Stadler, J. R., G. Goodwin and M. O. Creager, "A Comparison of Theory and Experiment for High-Speed Free-Molecule Flow," NACA Rept. 1032, 1951.
16. Seban, R. A., WADD-TR-60-370, Part II, August 1962.
17. Devienne, F. M., "Low Density Heat Transfer," Adv. Heat Transfer 2, Academic Press, 1965, pp. 272-356; Schafer, K., W. Rating and A. Eucken, Ann. Physik [5] 42, 176 (1942).

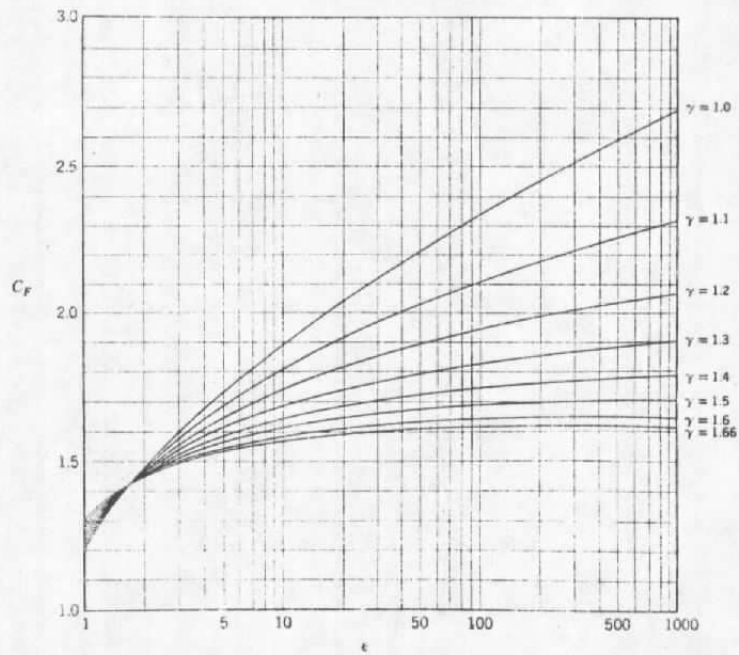
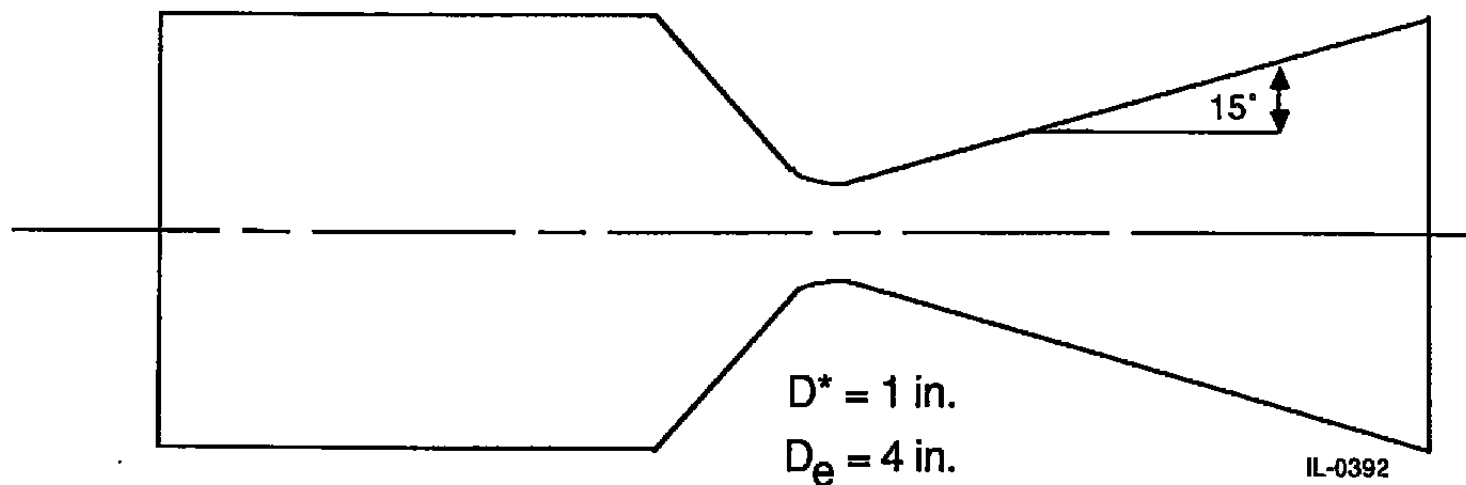


Figure 1. C_F versus ϵ for lossless nozzle in vacuum, with γ as a parameter. From Ref. 1.



$$P_0 = 10 \text{ torr}$$

$$T_0 = 500 \text{ K}$$

Gas: Carbon Dioxide

$$M_Q = 4$$

$$T_Q = 119 \text{ K}$$

$$P_Q = .063 \text{ torr}$$

$$n_Q = 5.85 \times 10^{21} / \text{m}^3$$

$$n_{\text{wall}} = 10^{21} / \text{m}^3$$

$$\lambda_Q = 0.020 \text{ cm}$$

Figure 2. Nozzle test conditions.

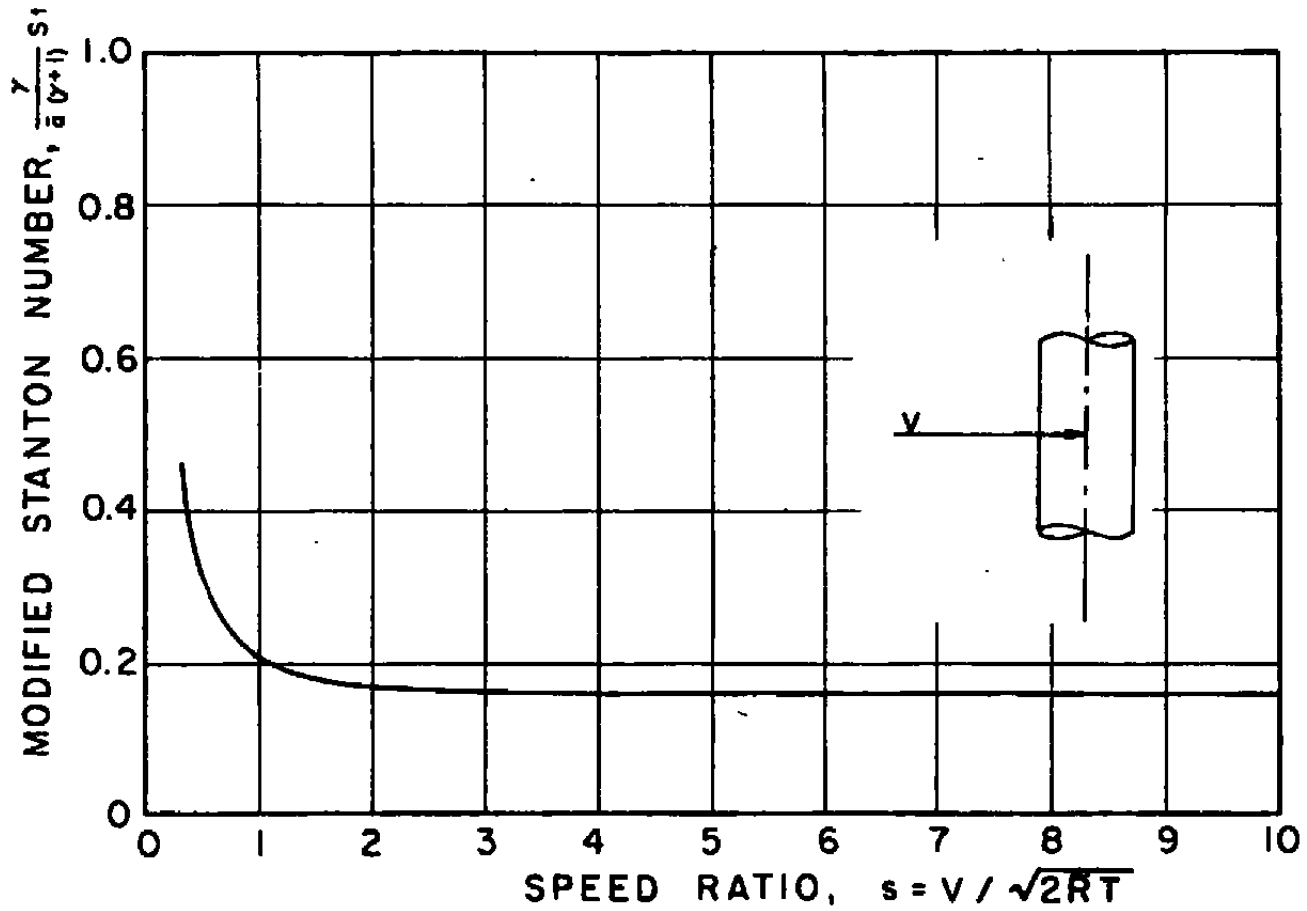


Figure 3. Modified Stanton number for a cylinder transverse to the flow direction in free molecular flow.

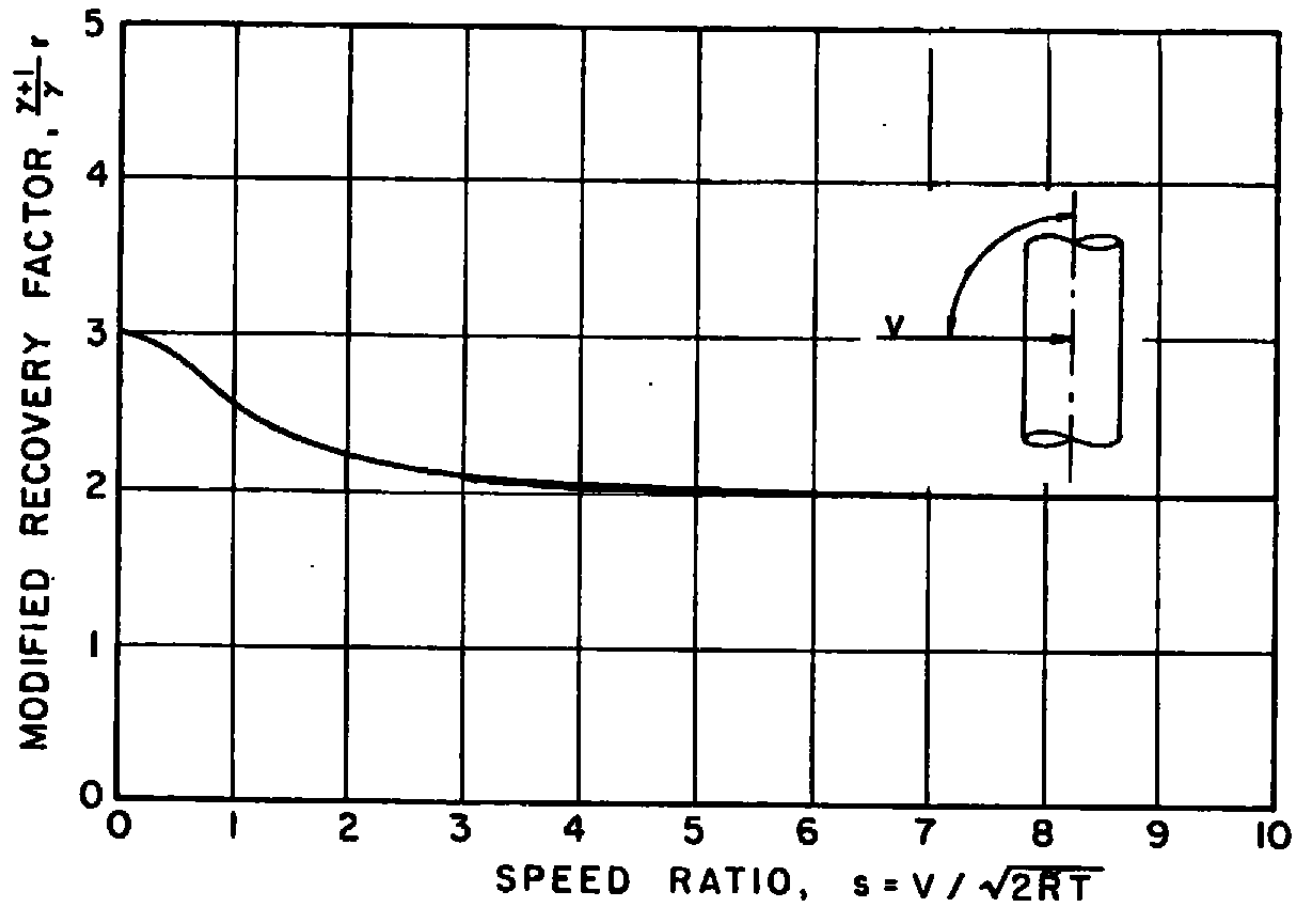


Figure 4. Modified recovery factor for a cylinder transverse to the flow direction in free molecular flow

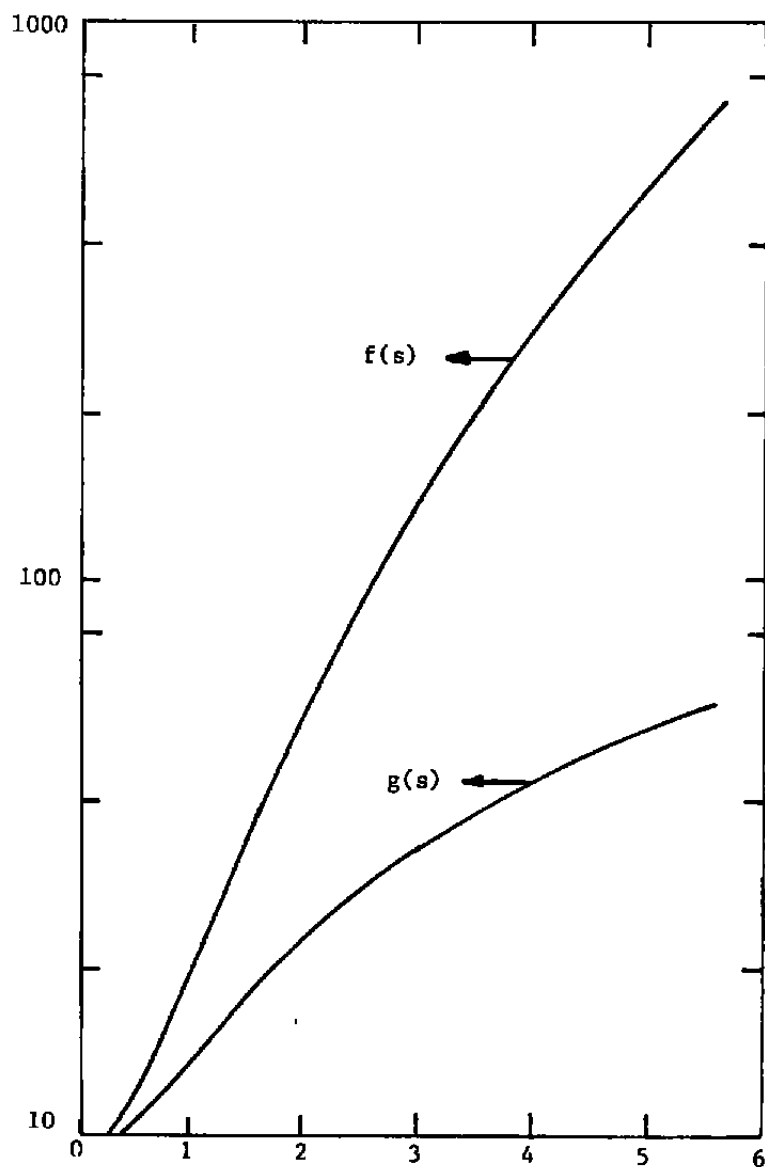


Figure 5. Functions $f(s)$ and $g(s)$ which appear in the expressions for the free-molecule heat transfer to a circular cylinder.

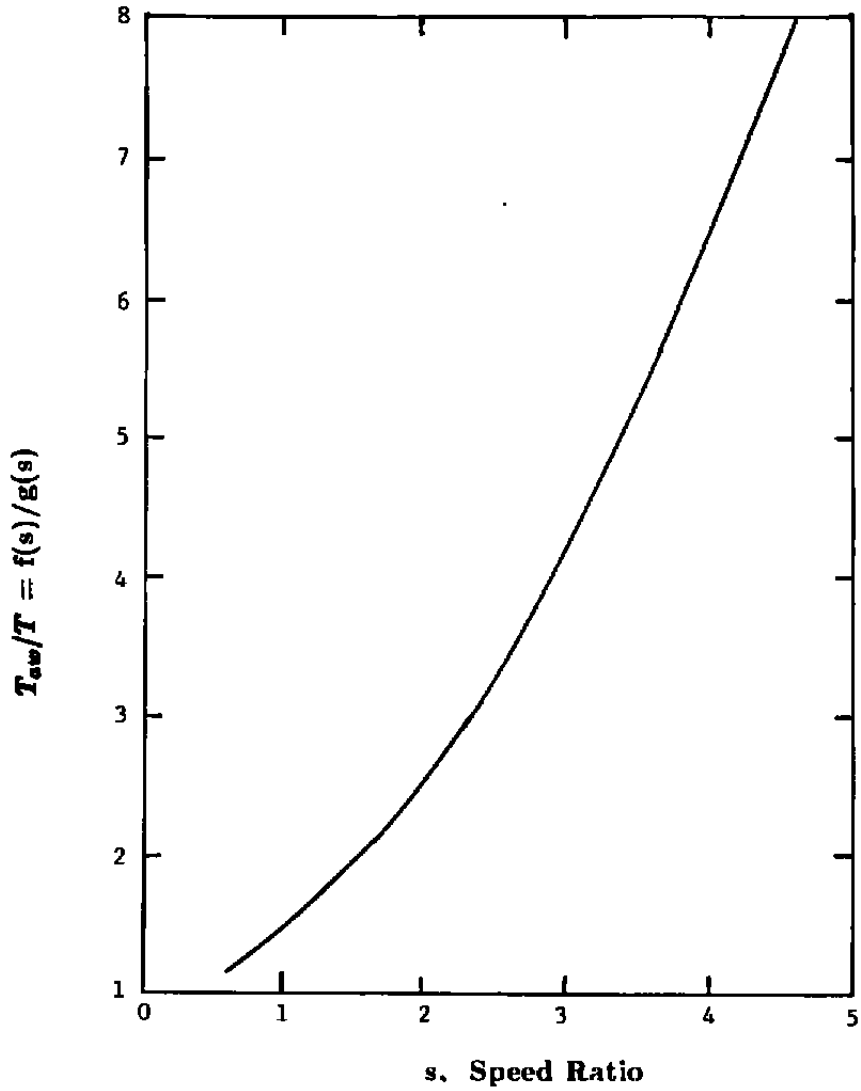


Figure 6. T_{aw}/T versus speed ratio for a circular cylinder in free-molecule flow.

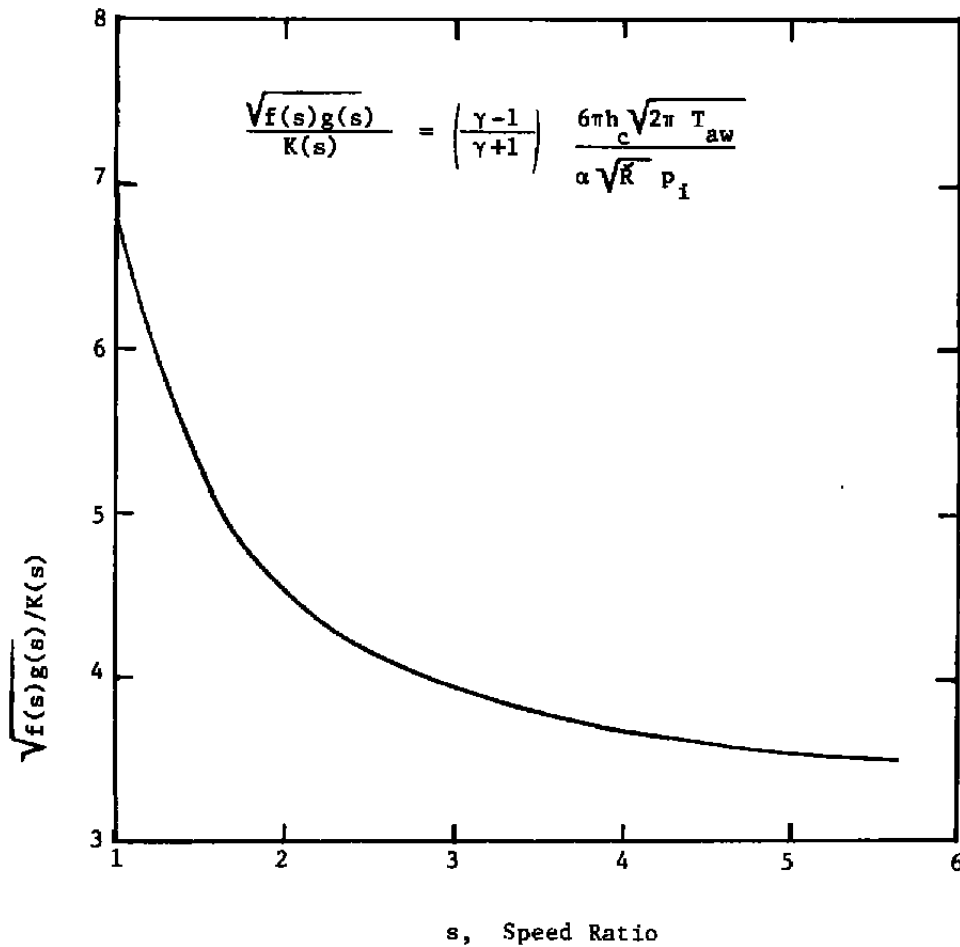


Figure 7. Function used by Muthoo and Brundin to determine speed ratio. From Ref. 13.

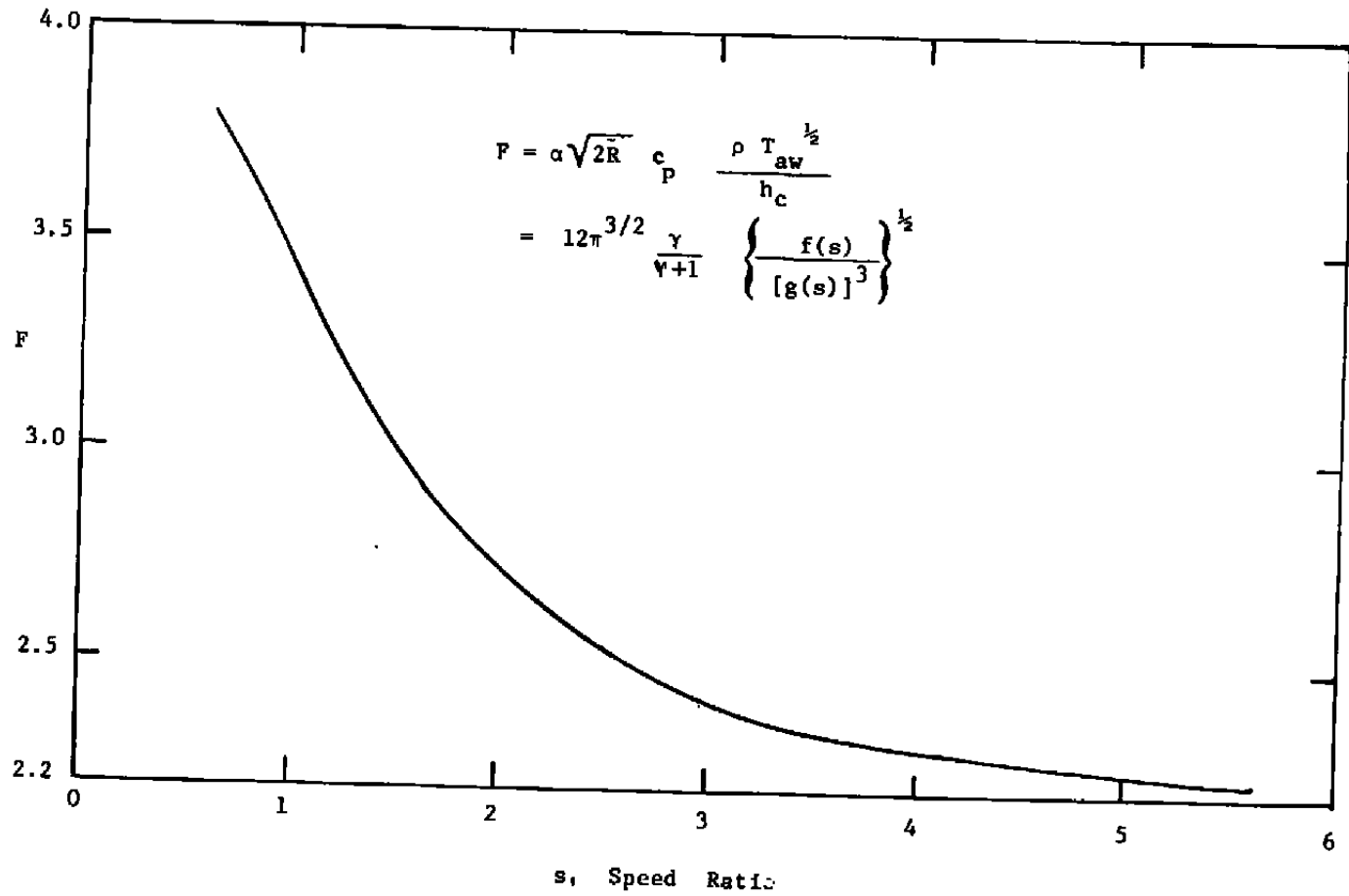


Figure 8. Function used by Gottediener (Ref. 2) to determine speed ratio.

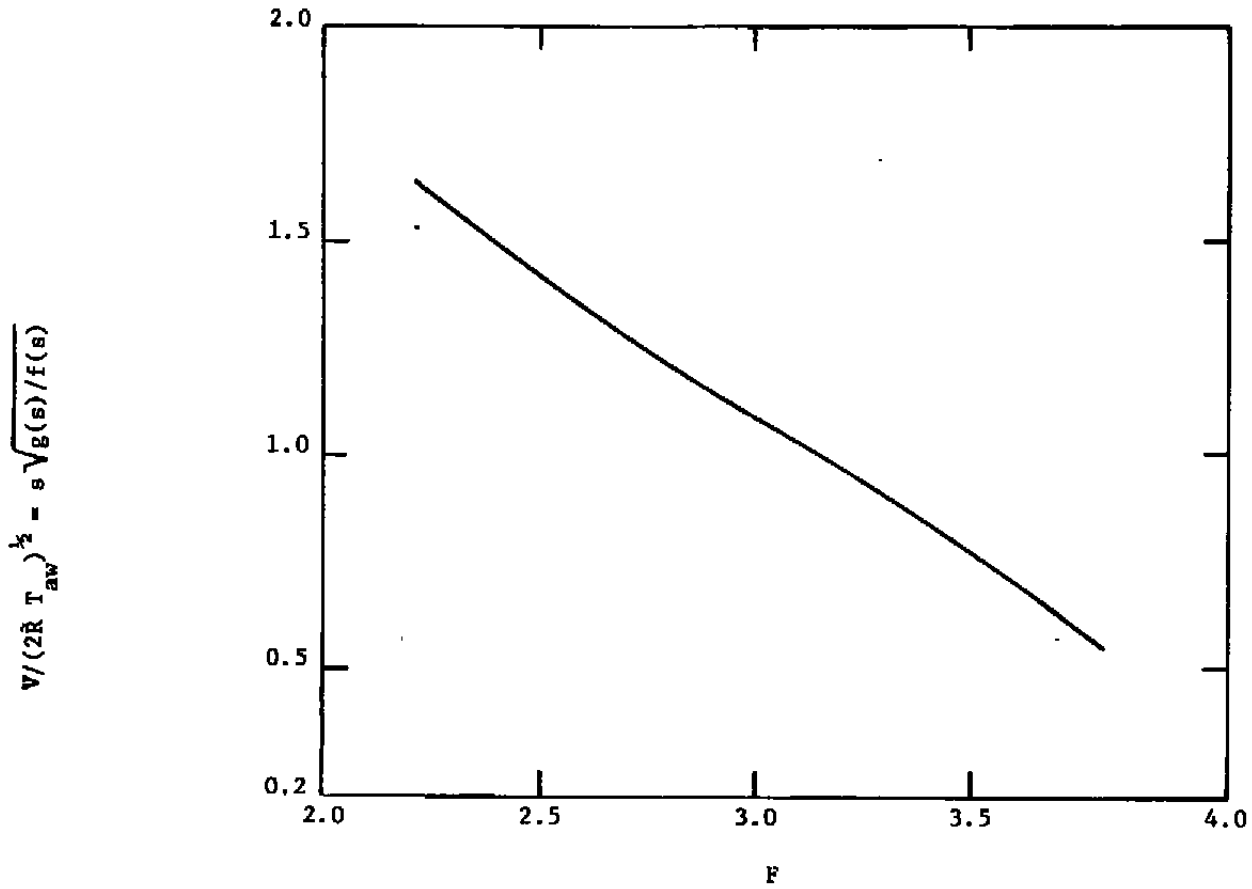


Figure 9. Relationship used by Gottesdiener (Ref. 2) to determine velocity.

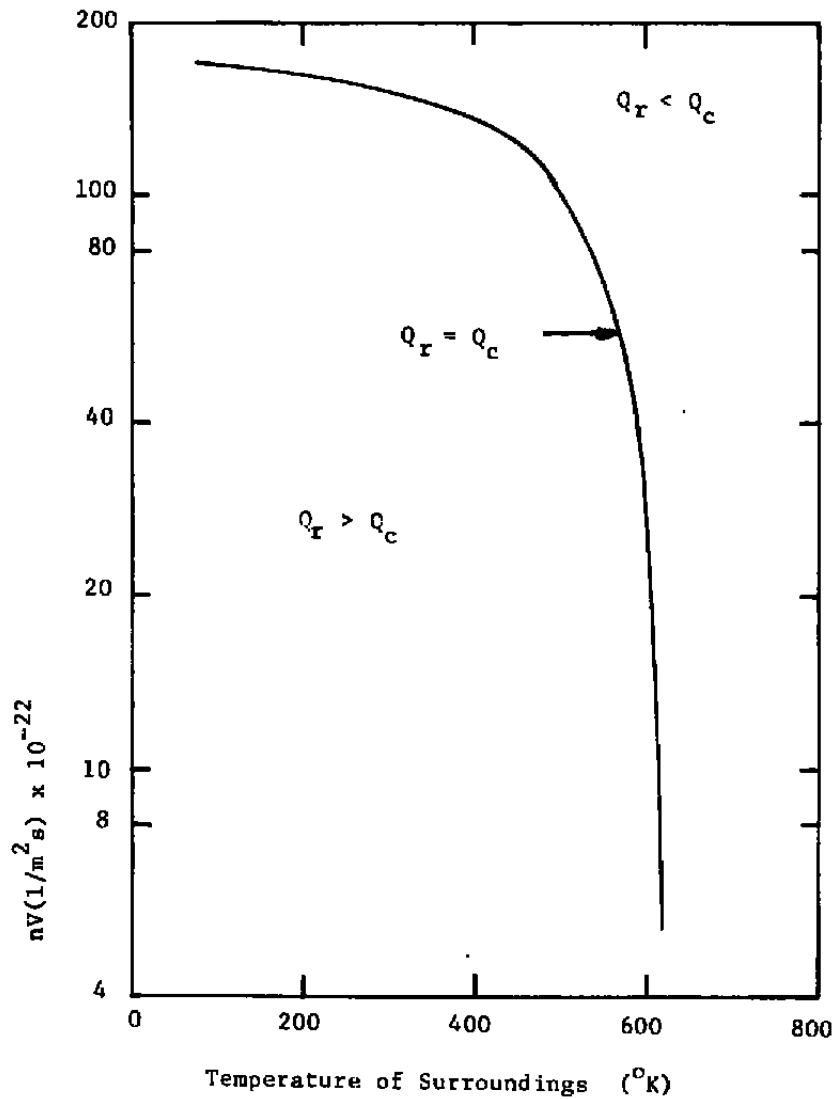


Figure 10. Comparison of convection (Q_c) and radiation (Q_r) heat transfer rates for the following conditions:
 $T_0 = 500^{\circ}K$, $T_w = 625^{\circ}K$, $\gamma = 1.4$,
 $\epsilon_w = 0.1$, $\alpha = 0.9$, $s = 3.0$.

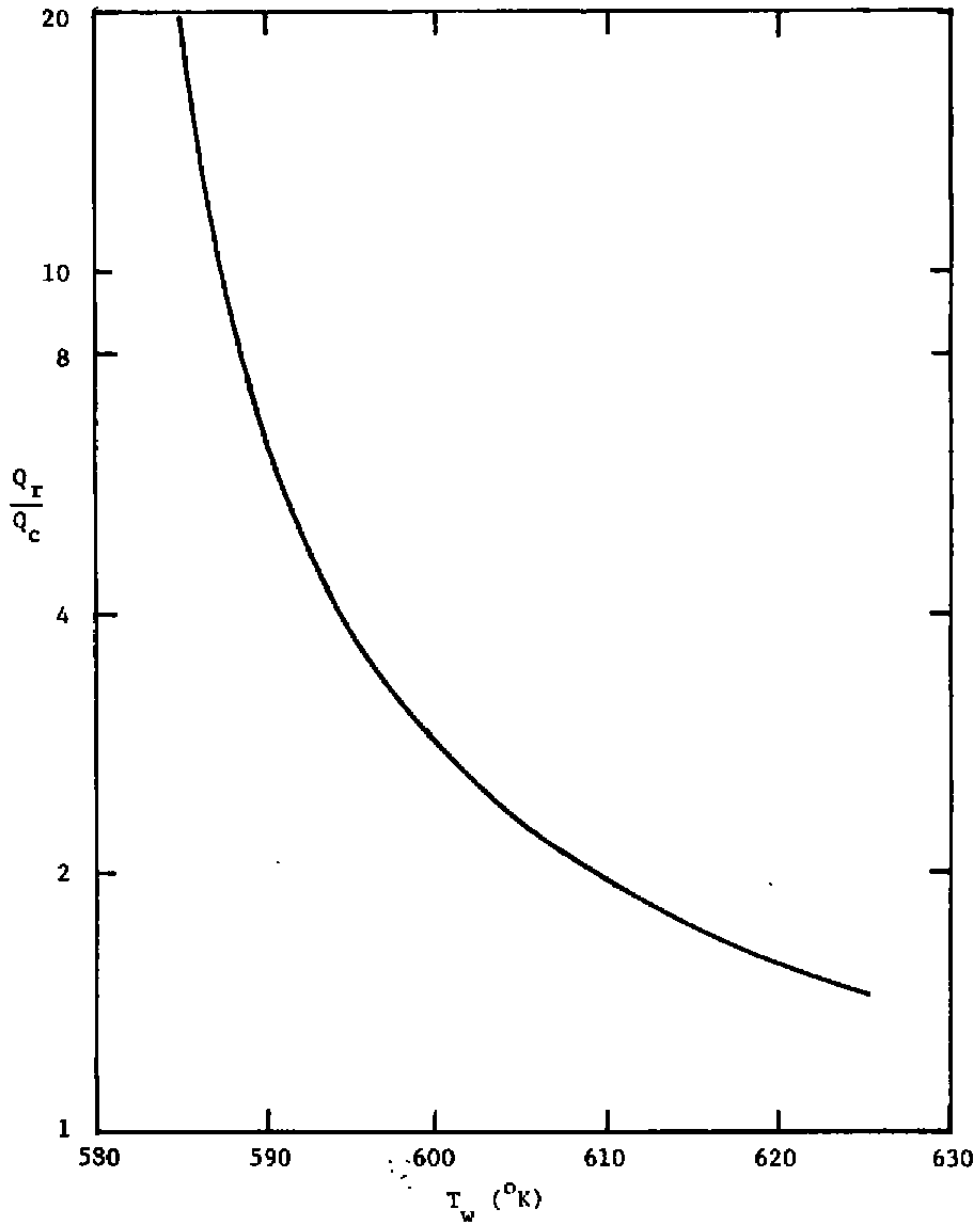


Figure 11. Q_r/Q_c for fixed $nV = 8 \times 10^{23}/\text{m}^2\text{s}$. $T_0 = 500^\circ\text{K}$,
 $\gamma = 1.4$, $\epsilon_w = 0.1$, $\alpha = 0.9$, $s = 3.0$.

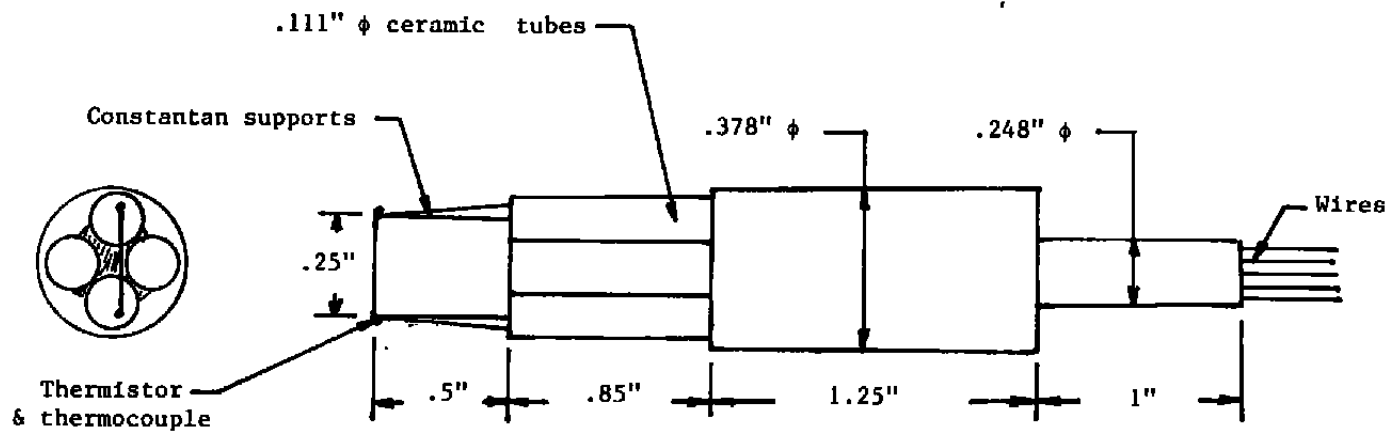


Figure 12. Construction of hot wire probe.

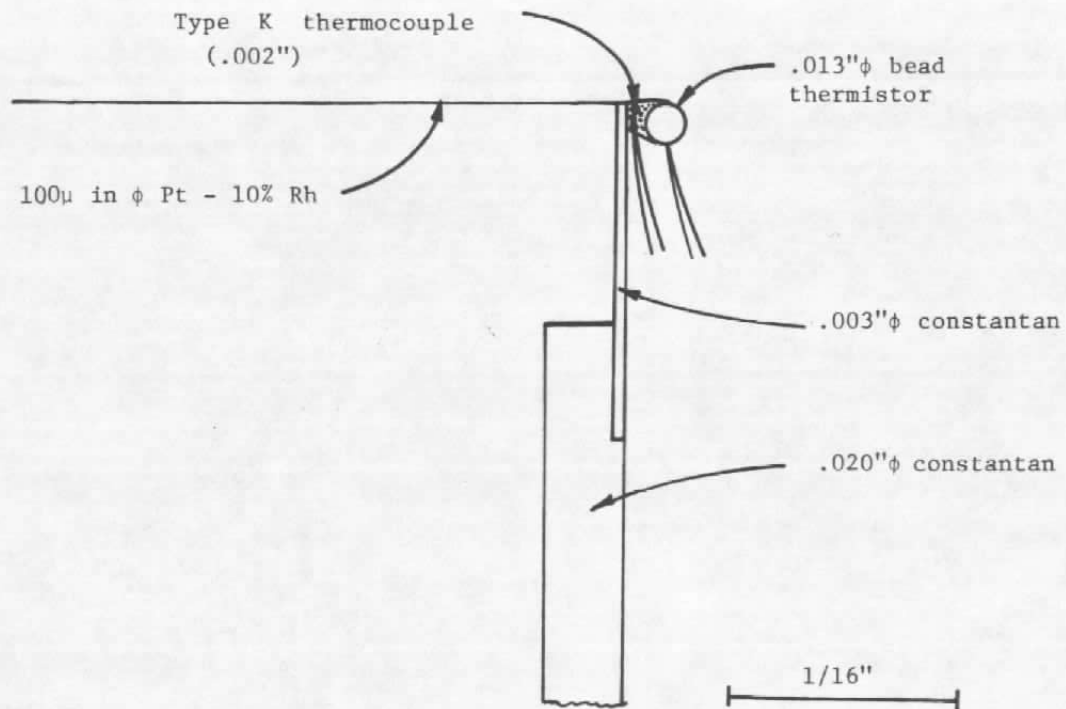
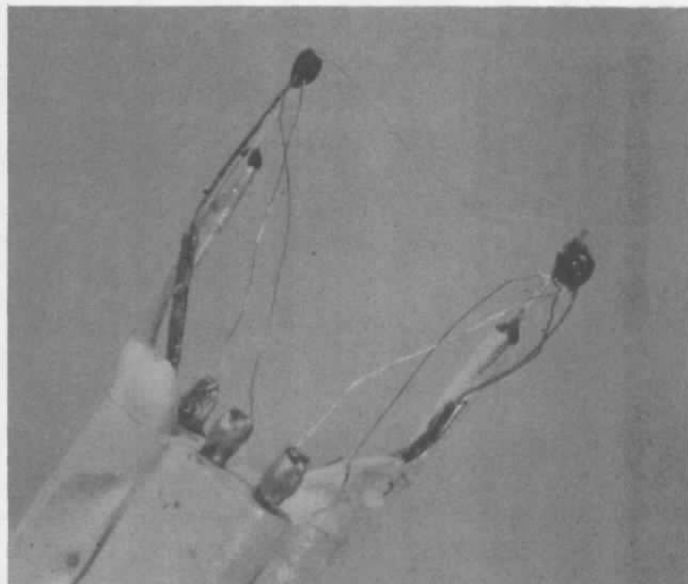
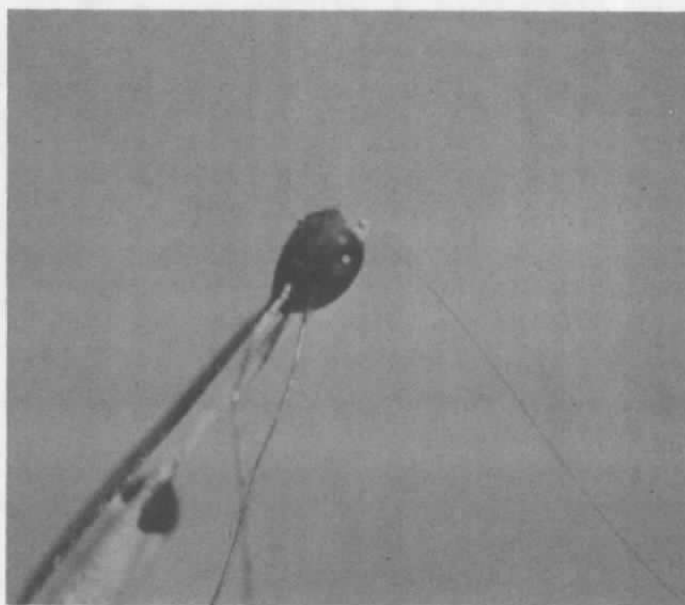


Figure 13. Detail of connections at end of wire.



a) Hot wire probe.



b) Close-up view of one end.

Figure 14. Microphotographs of free-molecule hot wire probes.

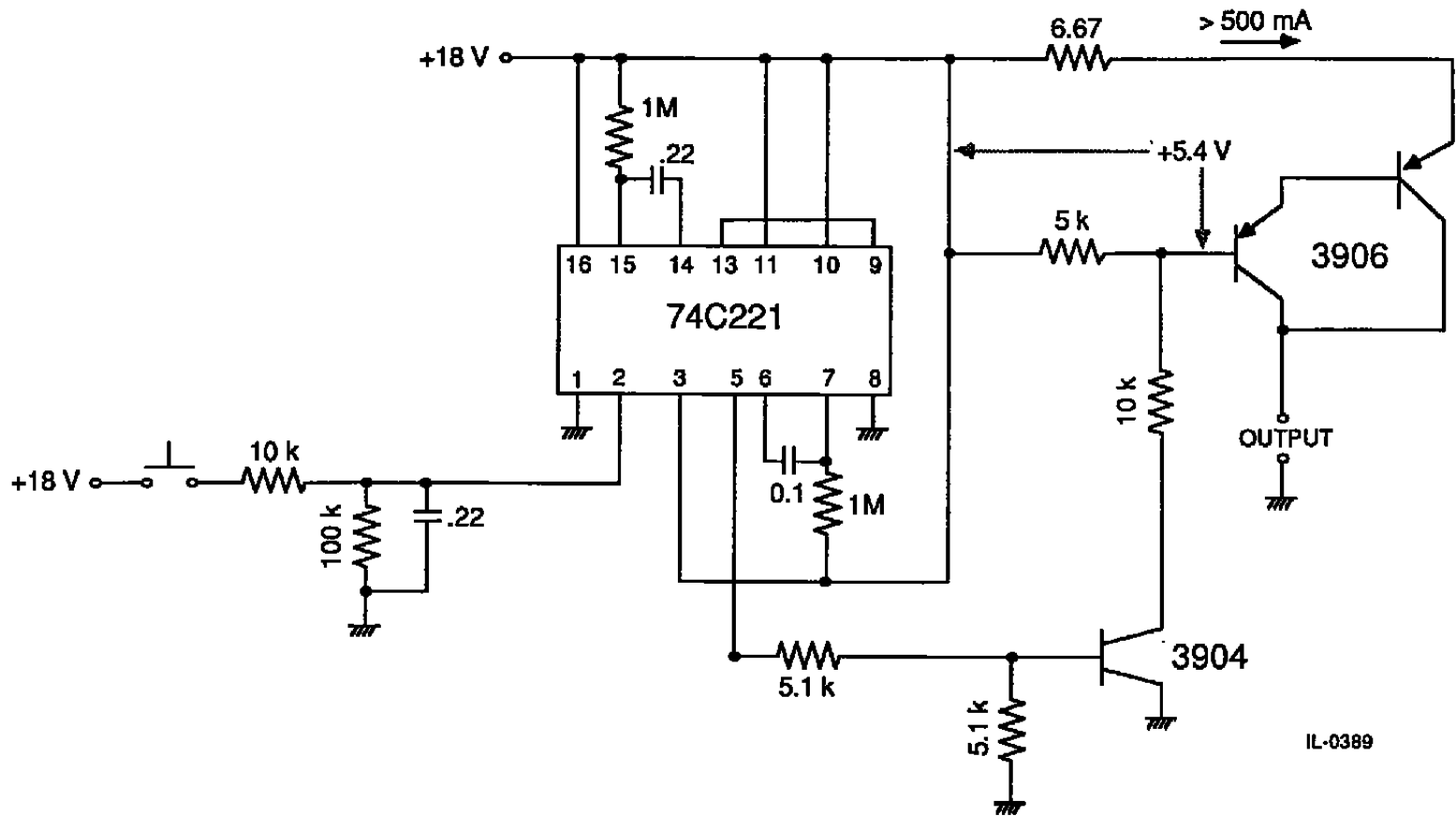


Figure 15. Spot welder used to attach wire to support posts.

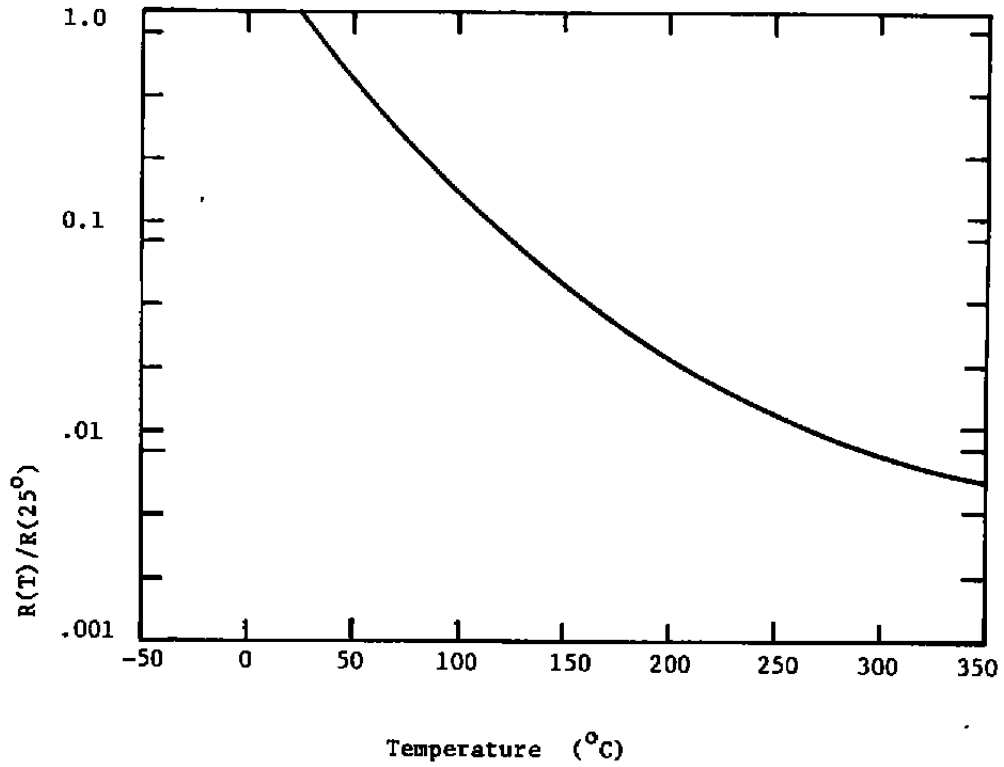


Figure 16. Resistance-temperature characteristic of glass-coated thermistors manufactured by Victory Engineering Corporation.

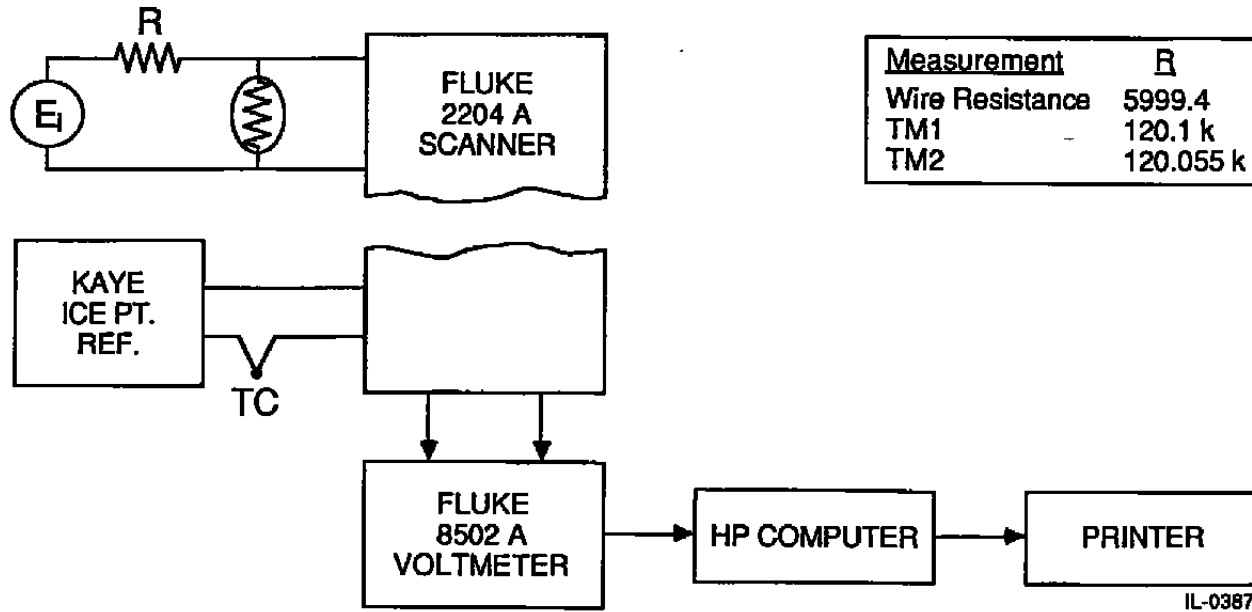


Figure 17. Probe calibration equipment.

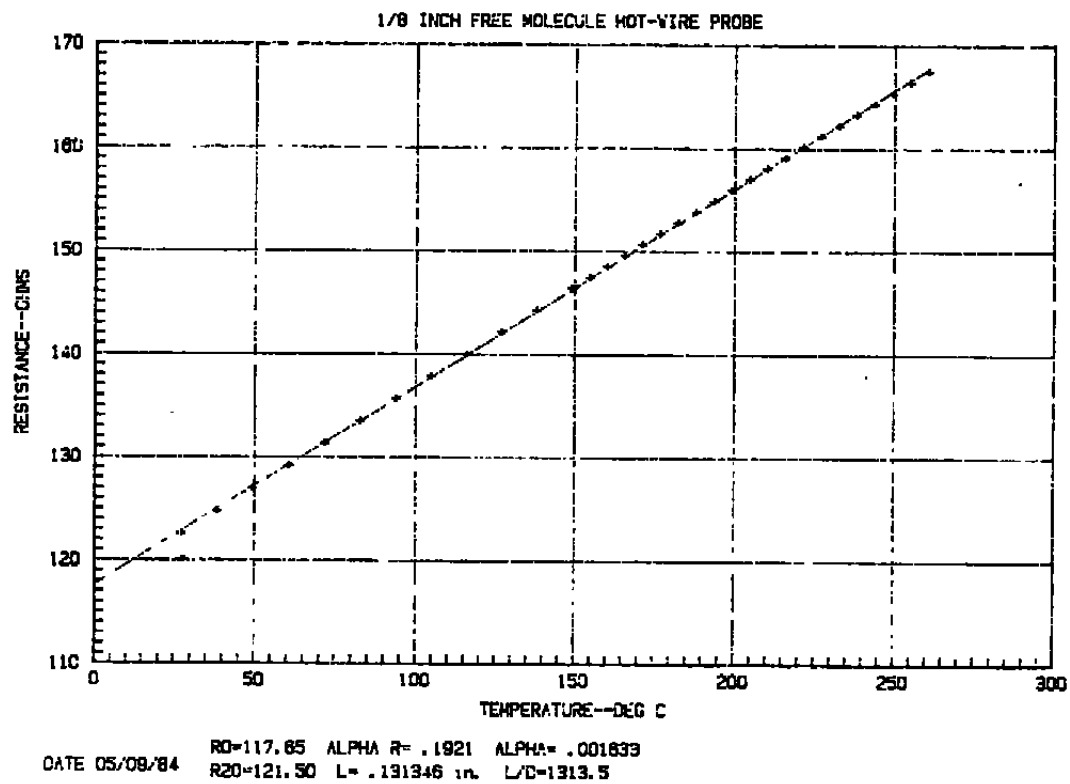
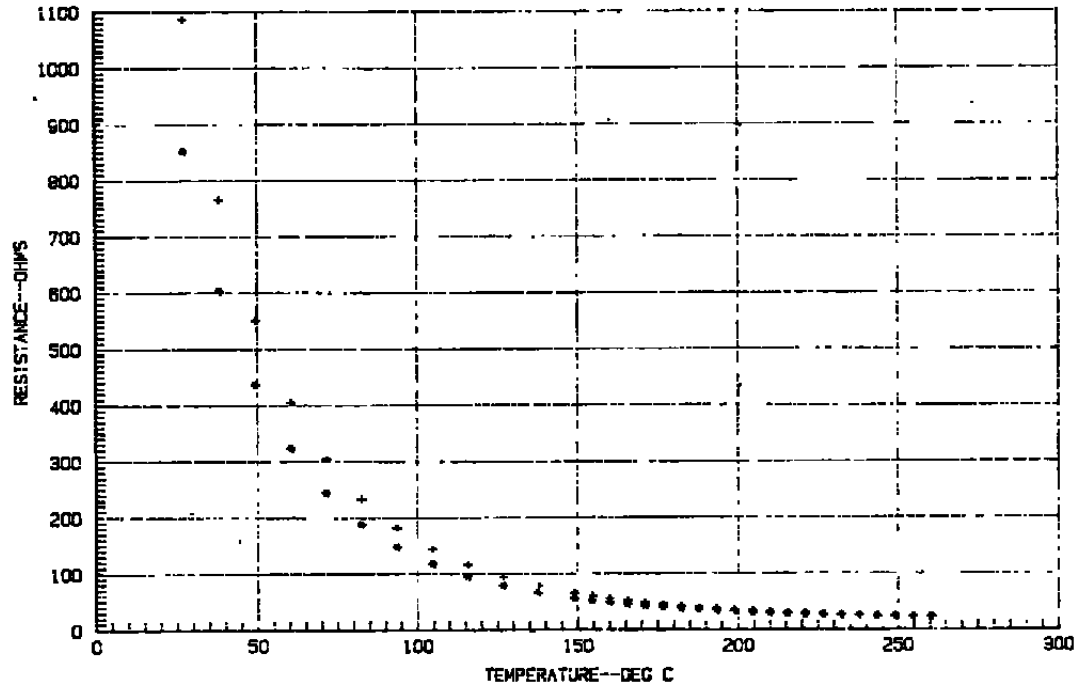


Figure 18. Measured resistance of 1/8 inch probe.



+ TN1
• TN2 9/9/84

Figure 19. Measured resistance of thermistors on 1/8 inch probe.

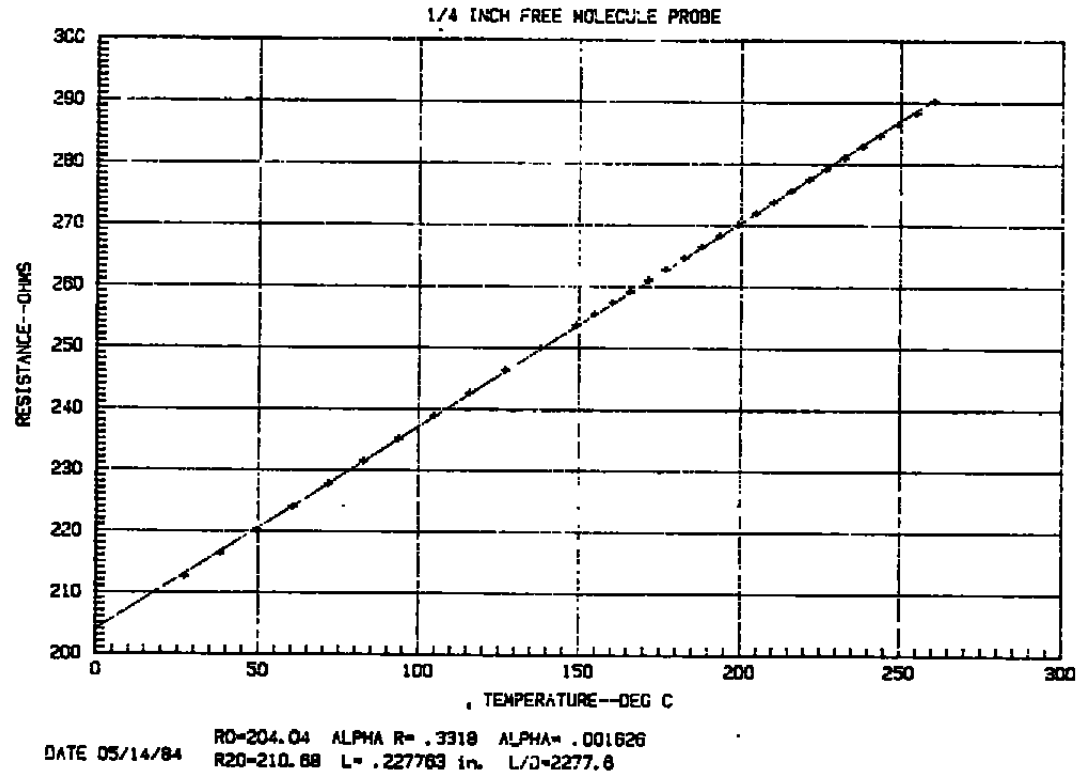
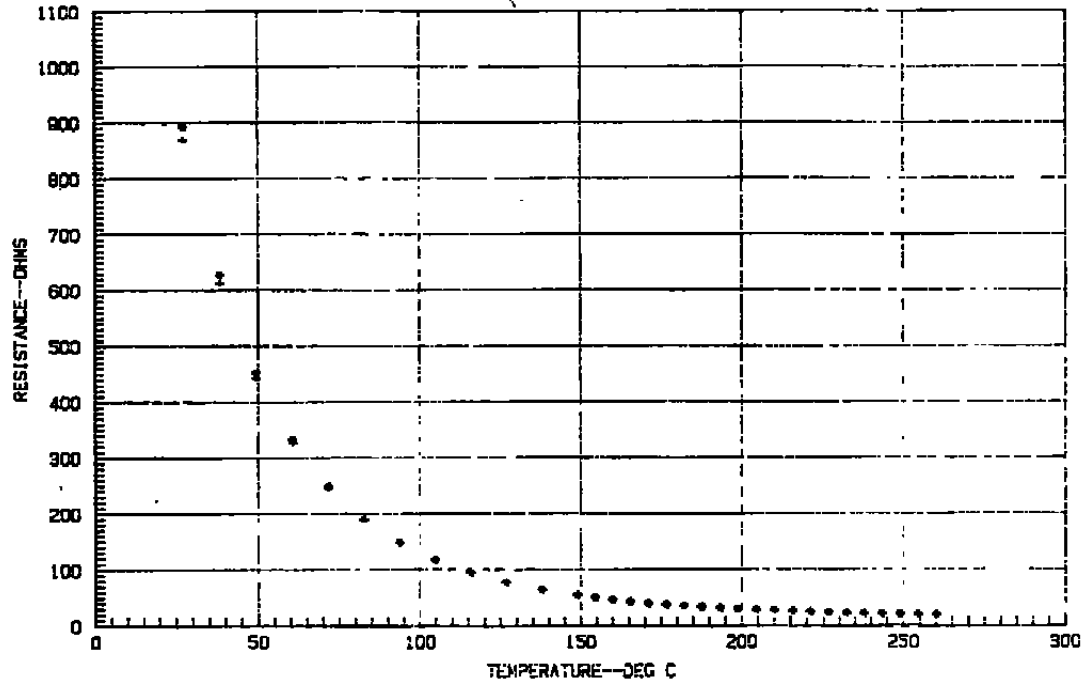


Figure 20. Measured resistance of 1/4 inch probe.



+ TML 5/14/84
o TML

Figure 21. Measured resistance of thermistors on 1/4 inch probe.

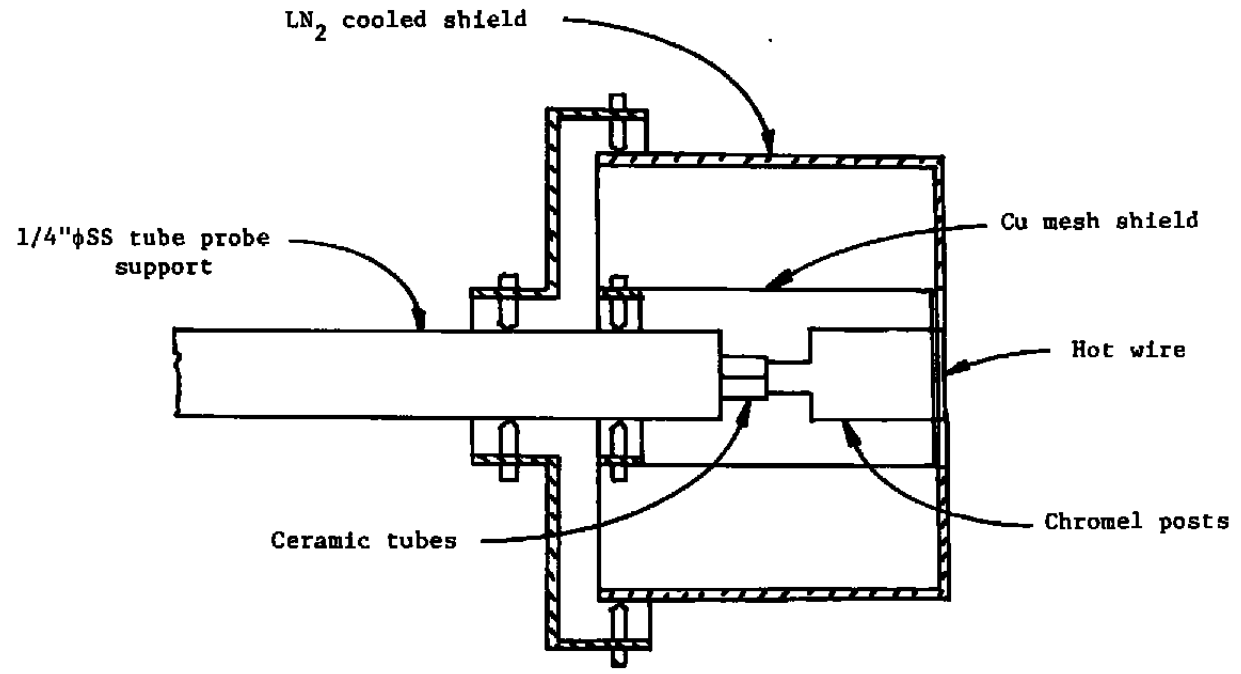


Figure 22. Probe radiation shield.

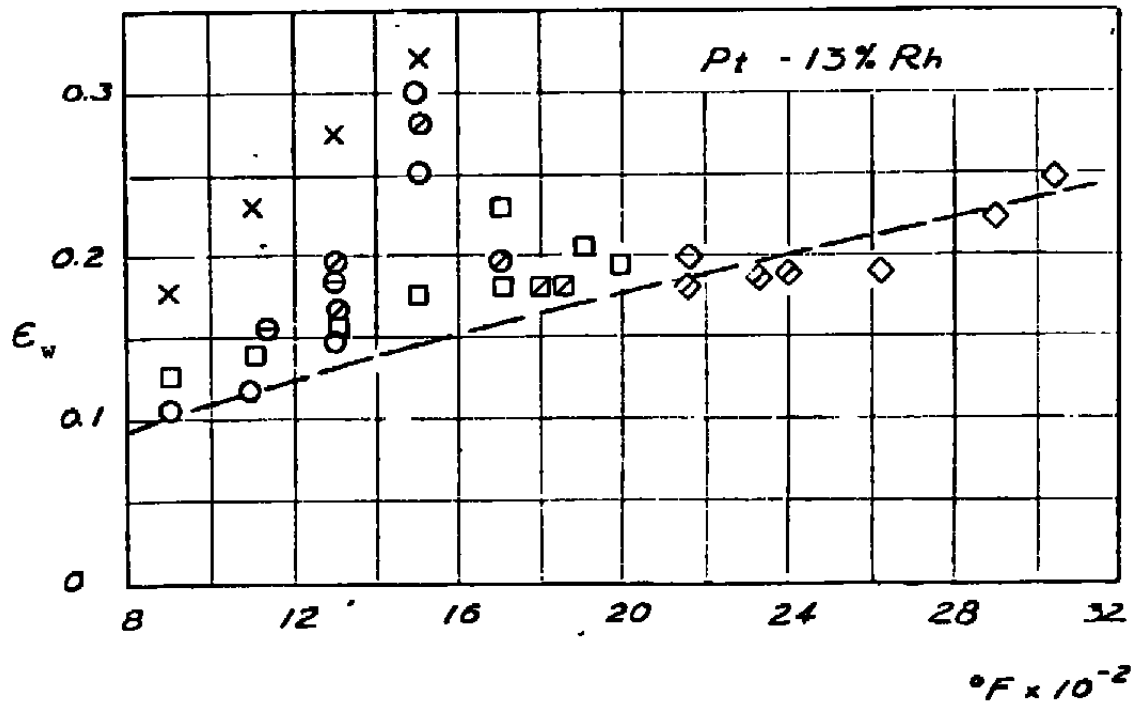
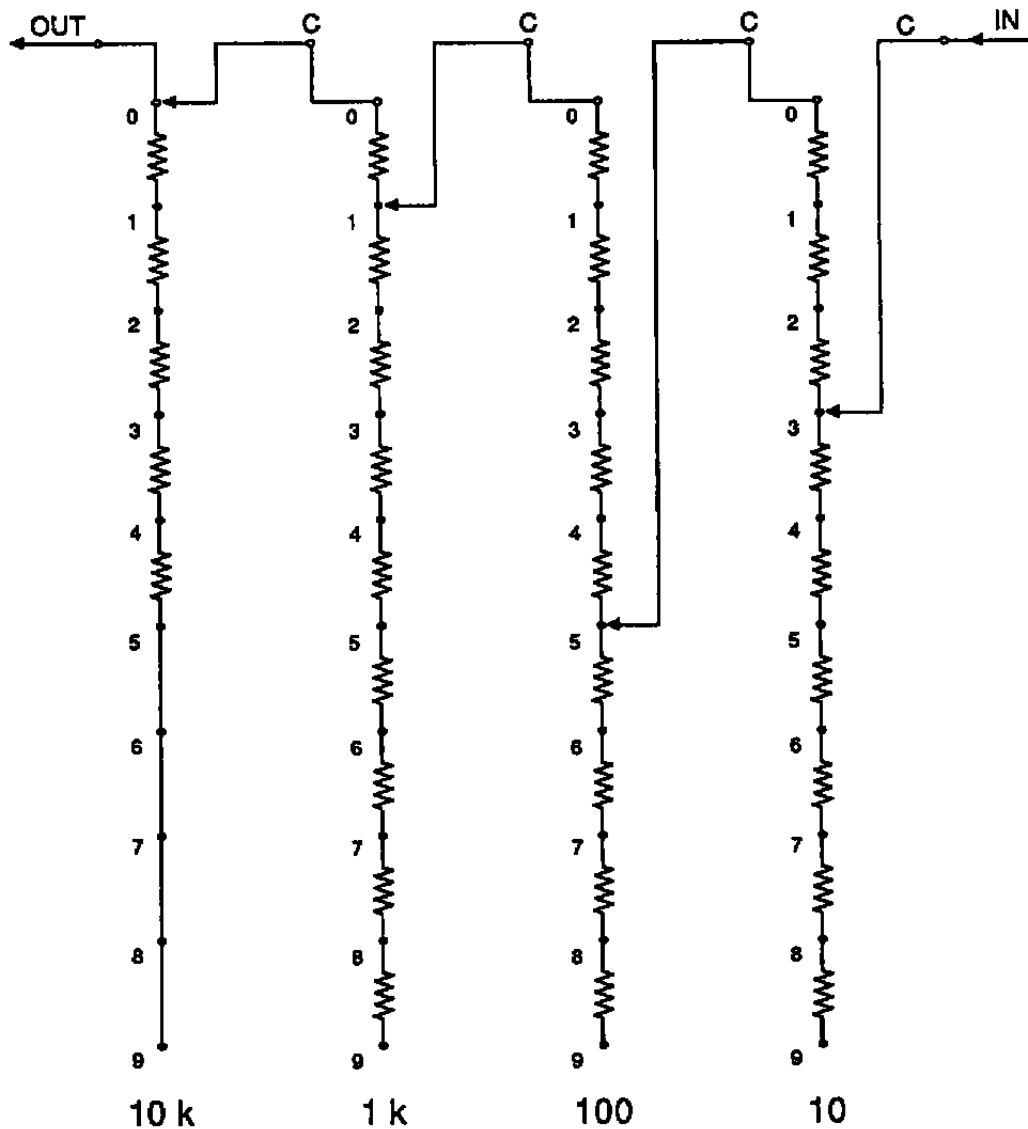


Figure 23. Total emittance of platinum 13% rhodium alloy (Ref. 16).



IL-0388

NOTES:

1. The decade switch is constructed from four, 10 digit thumbwheel switches.
2. The numbers to the left of the resistors indicate the value that R_w assumes when the switch is in that position.
3. All bridge resistors are metal film, $\pm 1\%$, ± 50 ppm / $^{\circ}\text{C}$, 1/10 watt.

Figure 25. Bridge decade resistor.

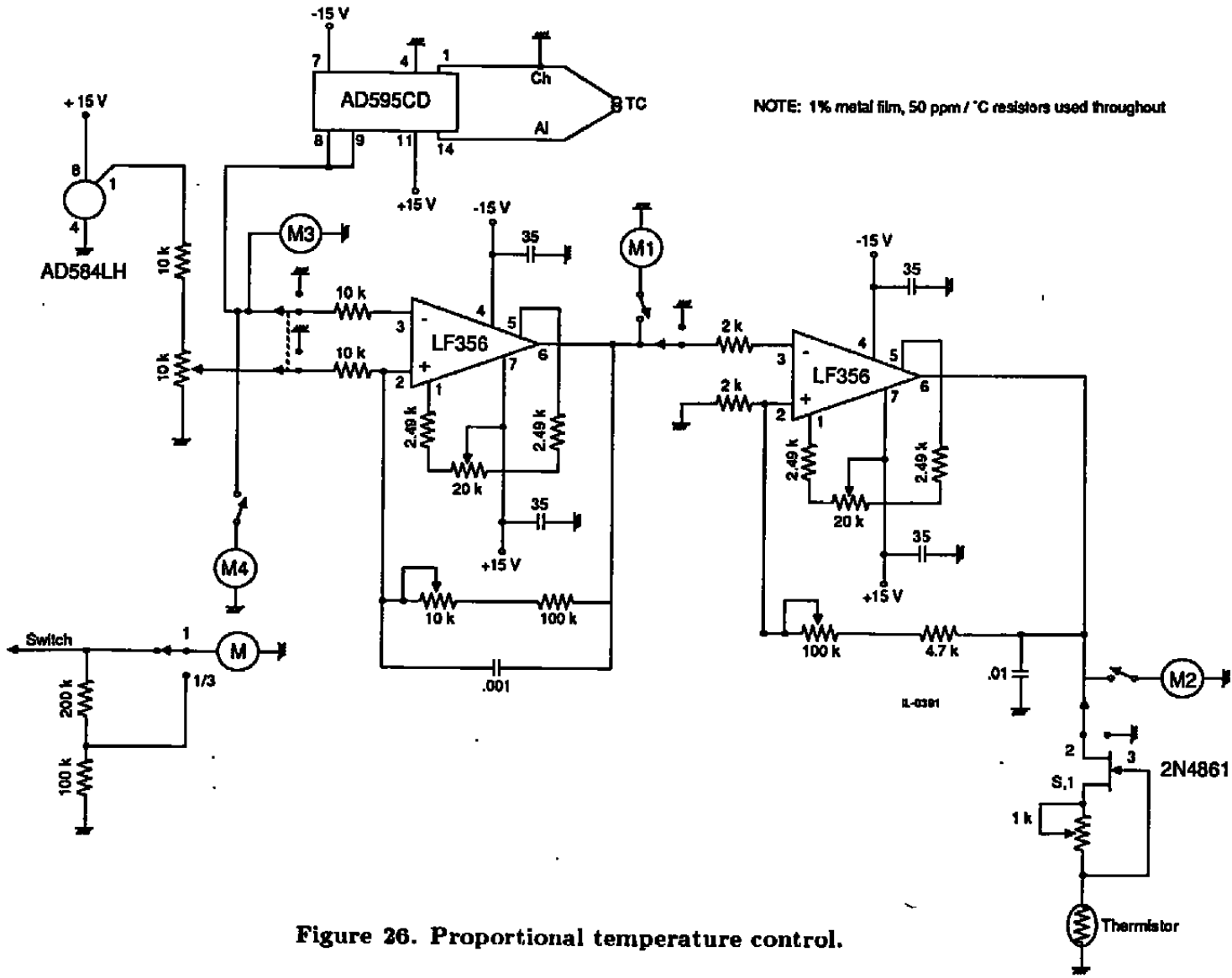


Figure 26. Proportional temperature control.

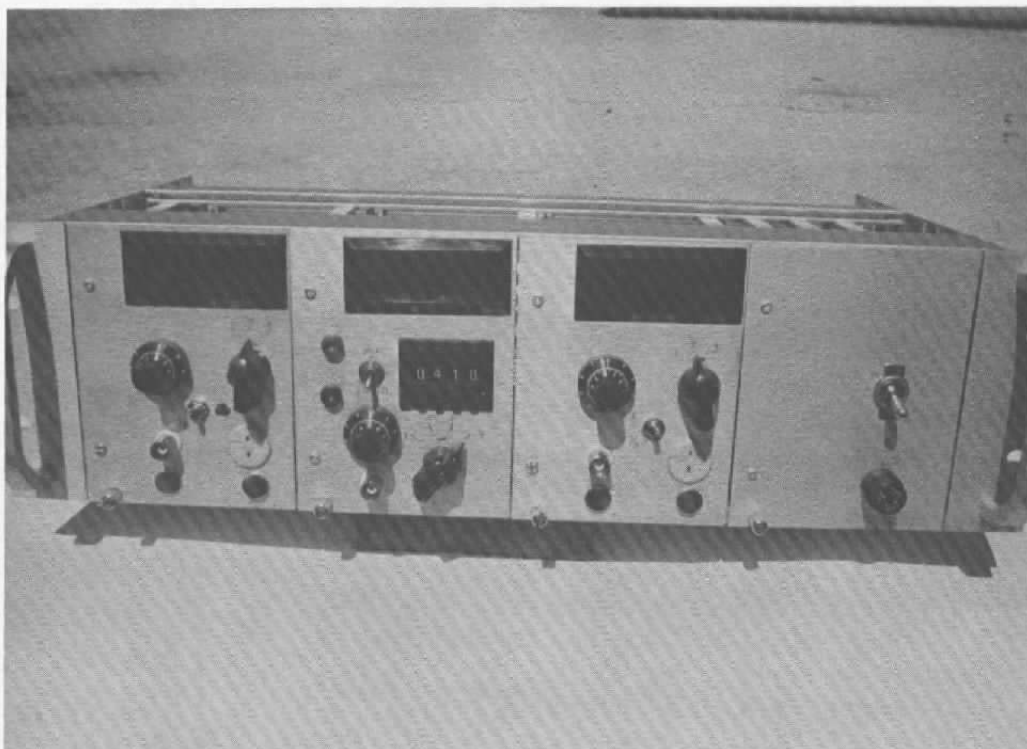


Figure 27. Photograph of free-molecule heat transfer probe electronics.

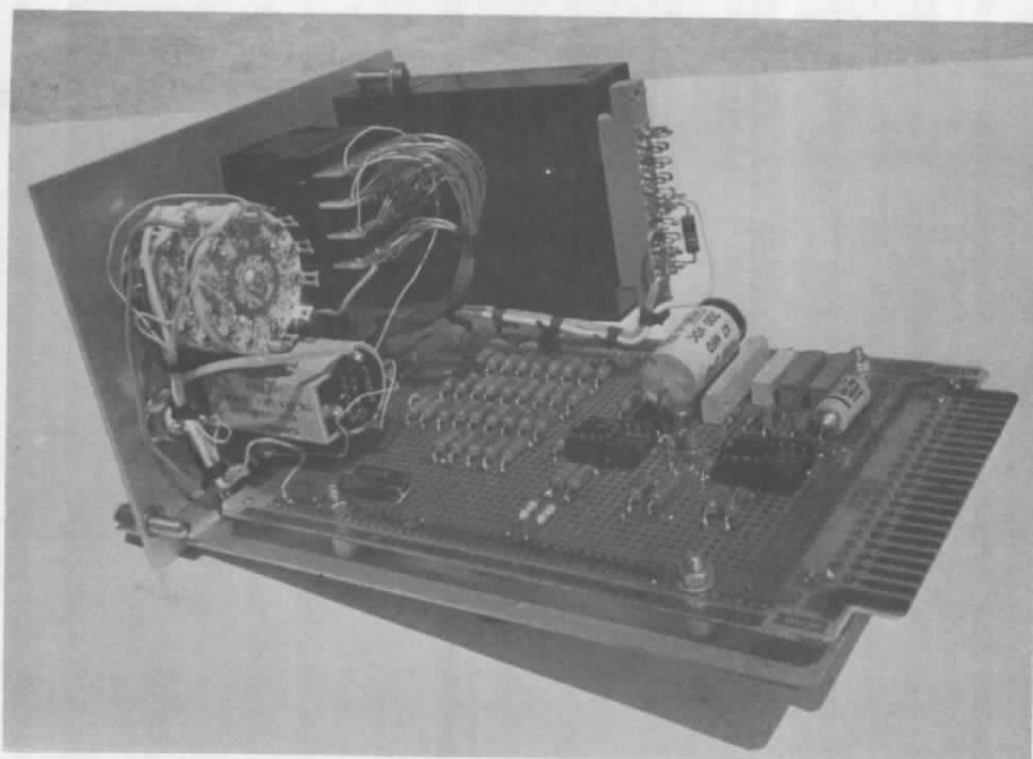


Figure 28. Photograph of hot wire control module.

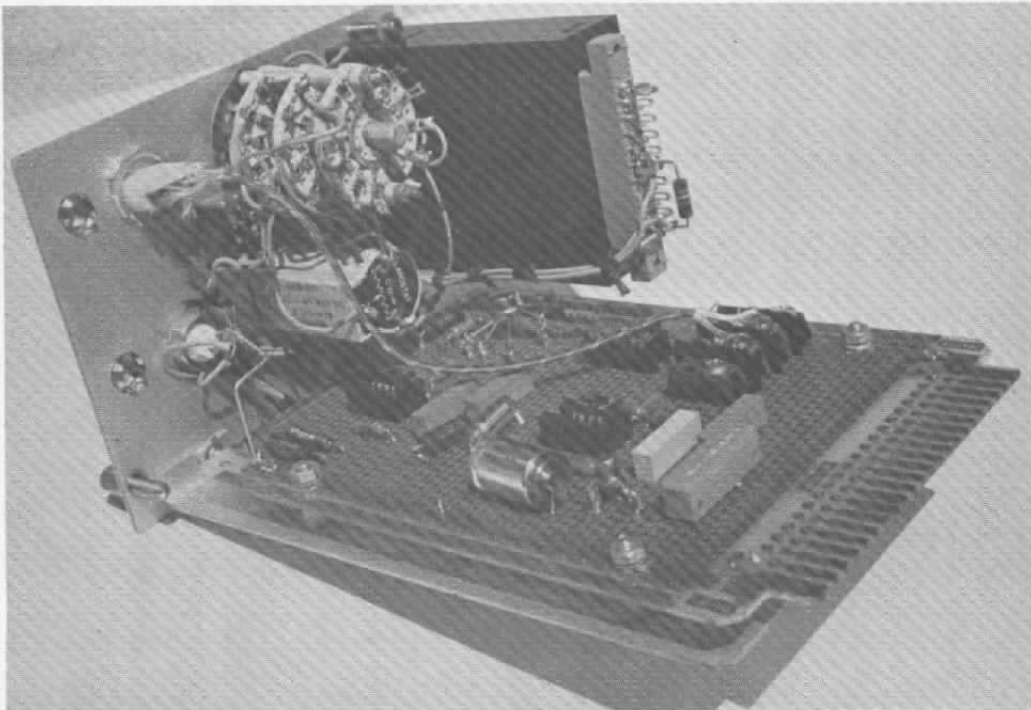


Figure 29. Photograph of proportional temperature controller module.

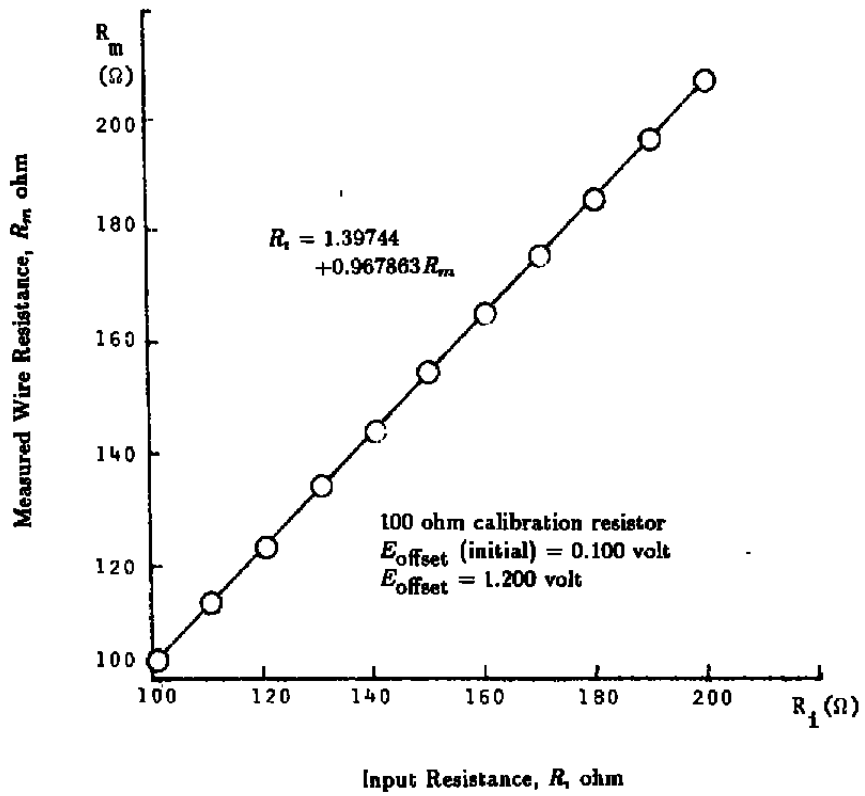
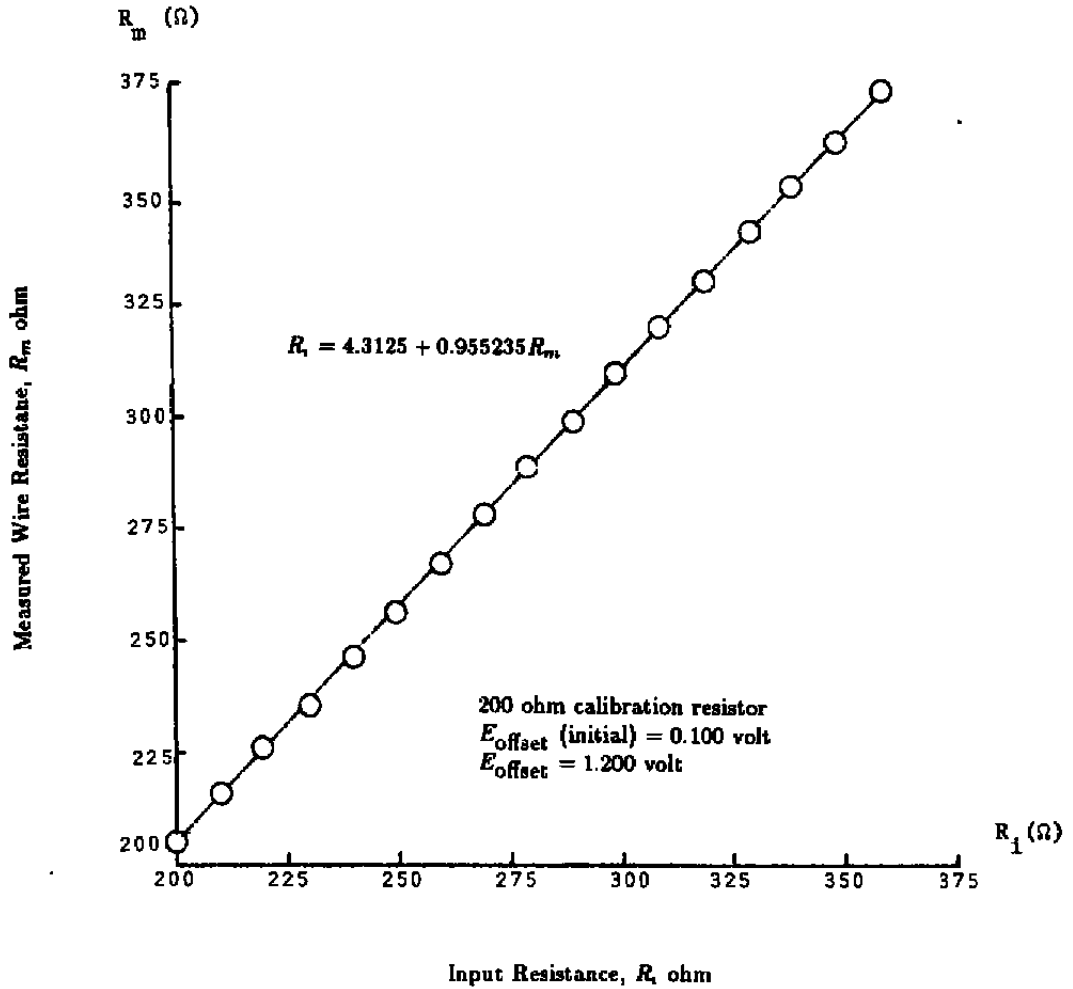


Figure 30. Bridge calibration.



! Figure 31. Bridge calibration.

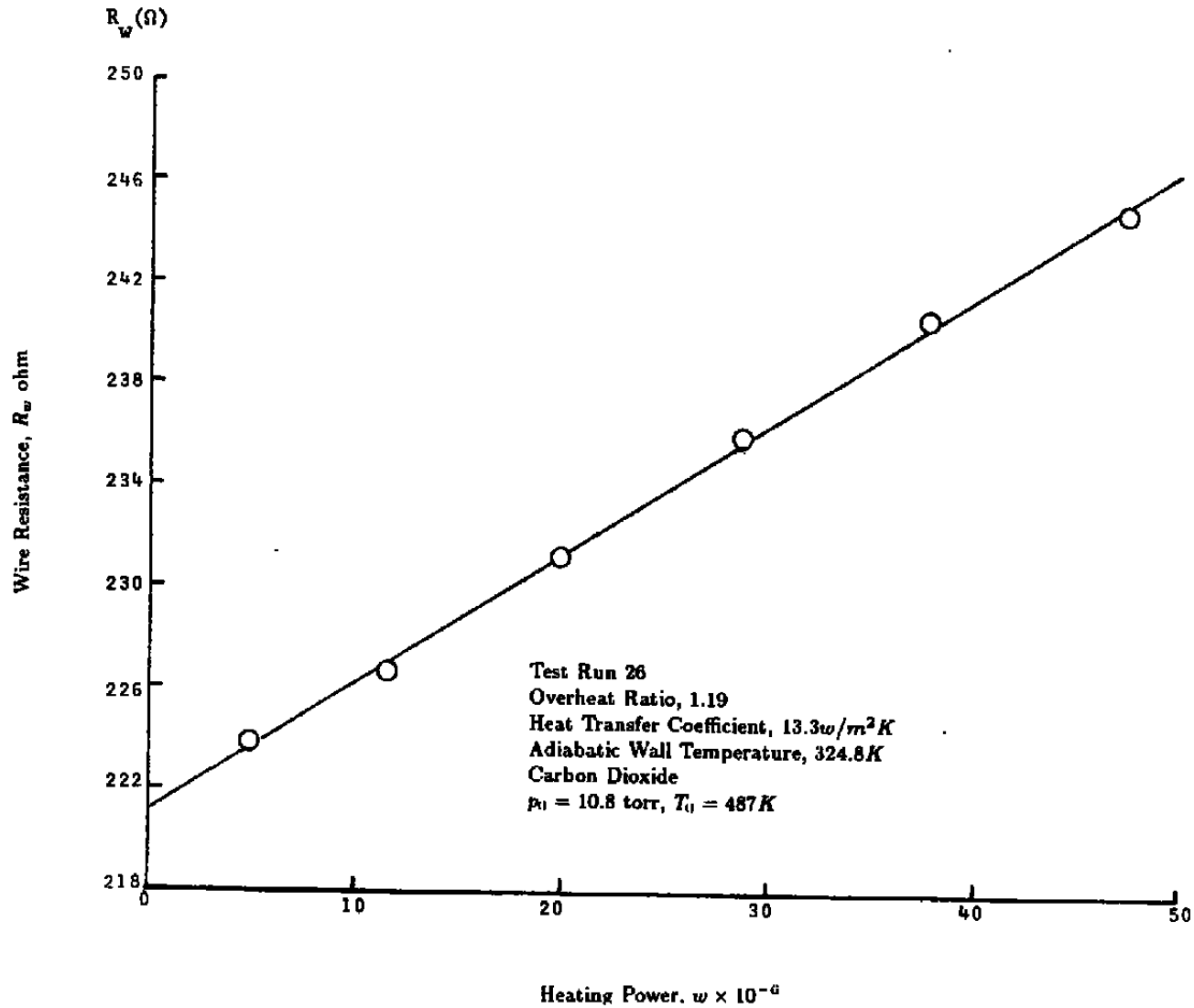


Figure 32. Probe measurements for probe outside plume shear layer.

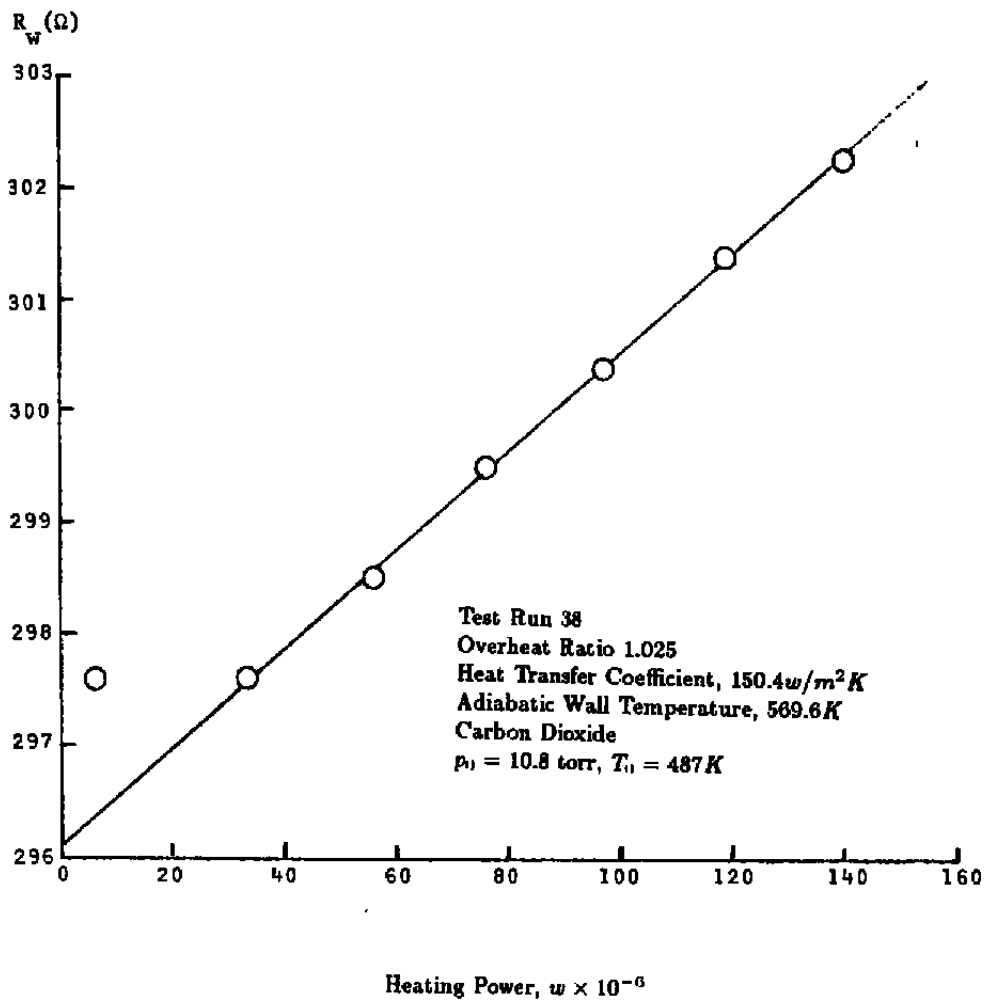
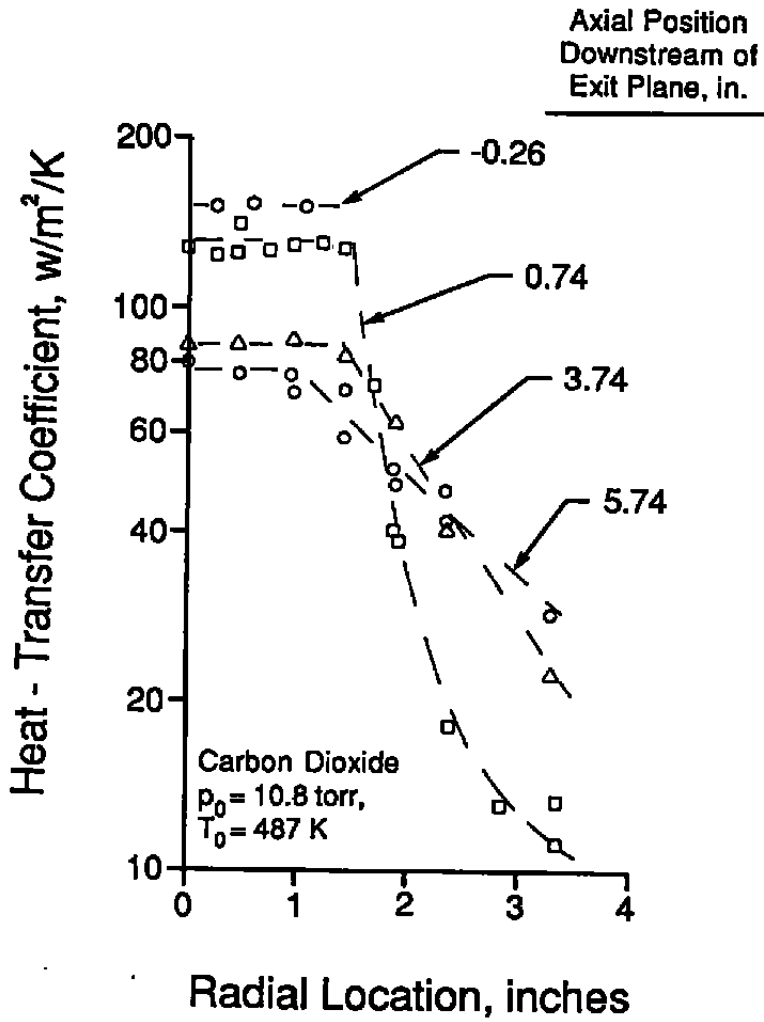
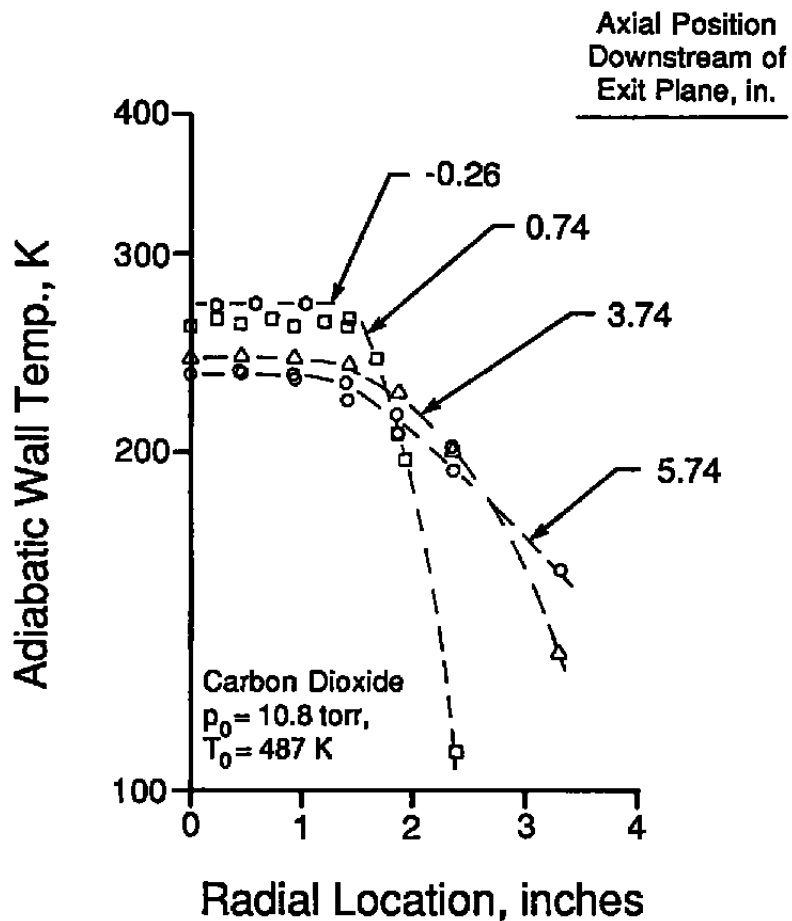


Figure 33. Probe measurements for probe inside nozzle.



CG-0789

Figure 34. Radial profiles of heat transfer coefficient measured by hot wire probe.



CG-0790

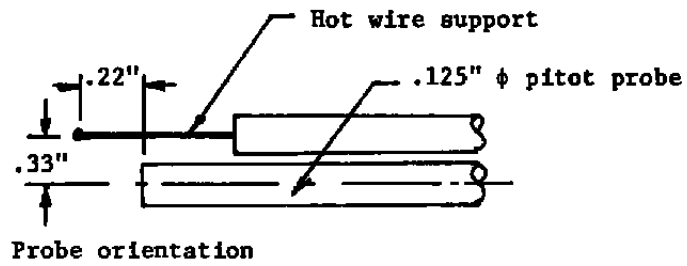
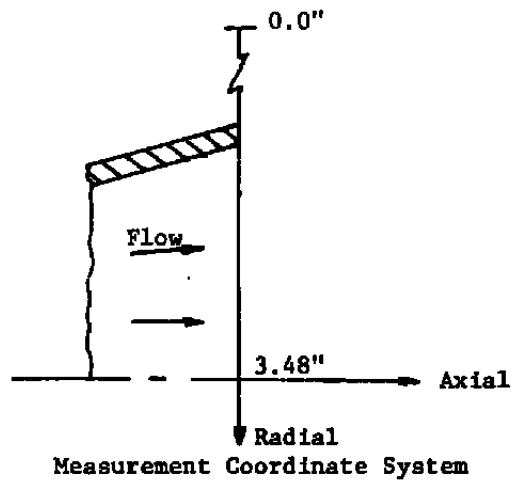
Figure 35. Radial profiles of adiabatic wall temperature measured by hot wire probe.

Table I
Operating Parameters of Hot Wire

Run Number	Lowest Overheat		Highest Overheat	
Run#	Wire Resistance (Ω) $R_i(\text{low})$	Heating Power (10^{-6})watts $P_i(\ell)$	Wire Resistance (Ω) $R_i(\text{high})$	Heating Power (10^{-6})watts $P_i(h)$
01	271.0	5.8	286.1	099.1
02	277.1	5.8	288.5	096.8
03	281.4	5.9	290.9	098.7
04	284.8	6.0	293.3	107.4
05	285.7	6.0	293.3	103.2
06	285.4	6.0	295.7	126.3
07	286.2	6.0	294.7	114.6
08	285.7	6.0	291.8	086.2
09	283.3	6.0	290.9	089.4
10	279.5	5.9	289.9	097.0
11	274.8	5.9	288.5	102.2
12	261.0	5.6	271.8	055.1
13	251.0	5.5	259.8	035.7
14	274.8	5.9	286.1	081.5
15	282.9	6.0	293.3	112.3
16	287.6	6.0	294.7	107.2
17	289.0	6.1	297.6	137.2
18	288.0	6.1	297.6	135.9
19	288.6	6.0	297.6	135.8
20	288.6	6.0	297.6	135.8
21	294.3	6.2	299.5	139.4
22	294.3	6.2	299.5	131.3
23	294.3	6.1	299.5	131.1
24	294.8	6.3	299.0	118.6
25	276.4	5.9	288.5	088.5
26	223.8	4.9	245.5	047.5
27	222.4	4.9	245.5	047.6
28	221.2	4.9	243.1	047.7
29	221.2	4.9	247.9	055.9
30	227.6	5.0	250.3	049.7
31	242.9	5.3	262.2	057.3
32	272.1	5.8	288.5	101.1
33	288.6	6.1	298.0	117.9
34	295.2	6.1	300.4	134.3
35	295.2	6.2	300.4	134.9
36	295.2	6.3	300.4	128.8
37	295.7	6.2	300.9	131.3
38	297.6	6.2	302.3	140.2
39	298.1	6.3	302.3	138.6
40	298.1	6.2	302.8	143.2
41	298.1	6.3	302.8	141.6

Table II
Hot Wire Measurements From Nozzle Tests

Run Number	Thermocouple Temperature (°C)	h_c (watt/m ² °K)	T_{aw} (°C)	Location	
				Axial (inch)	Radial (inch)
01	089.8	046.3	193.5	5.735	5.850
02	098.2	054.0	207.8		5.380
03	106.4	065.1	221.2		4.910
04	113.5	078.2	231.4		4.440
05	117.0	084.4	234.6		3.960
06	117.0	088.0	234.1		3.490
07	118.1	083.8	235.6		3.020
08	117.3	083.7	234.3		2.540
09	111.6	078.9	229.9		2.070
10	104.0	057.6	215.1		1.600
11	097.4	052.7	201.9		1.130
12	081.9	031.4	157.0		0.183
13	073.8	024.7	132.4	3.735	0.183
14	101.6	045.3	201.3		1.130
15	114.1	069.5	226.2		1.600
16	125.4	091.5	239.9		2.070
17	129.6	098.4	243.5		2.540
18	128.7	095.1	242.8		3.020
19	129.2	095.1	242.8		3.490
20	130.1	095.1	242.8		3.960
21	152.9	155.8	260.0	0.735	3.960
22	153.0	141.4	259.1		3.490
23	153.4	138.6	258.7		2.540
24	154.6	141.7	259.9		2.070
25	125.0	044.9	206.3		1.600
26	036.9	014.7	051.6		0.145
27	035.5	012.4	043.1		0.145
28	029.9	012.9	035.5	-0.260	0.145
29	030.0	013.4	039.6		0.620
30	046.4	014.4	061.8	0.735	0.620
31	068.3	019.8	107.9		1.090
32	105.7	042.4	196.7		1.560
33	138.1	080.1	243.4		1.800
34	151.5	144.0	261.5		2.040
35	152.6	144.5	261.6		2.270
36	152.9	139.5	261.9		2.740
37	153.7	136.6	262.5		3.220
38	165.9	166.8	269.4	-0.260	3.220
39	166.5	170.0	269.9		2.900
40	166.8	167.9	270.5		2.430
41	167.9	164.5	270.7		1.900



APPENDIX A

FREE-MOLECULE FLOW PROPERTIES DOWNSTREAM of a RECTANGULAR ORIFICE

The free-molecule heat transfer probe cannot be used to measure a flow field without an independent measurement of one flow variable, such as the density. However, if the density was known from theory for some flow, then the operation of the probe and the effectiveness of the radiation shields could be verified without the need for a companion instrument. The free-molecule flow through an orifice into a vacuum offers such a flow because all of the flow properties at any point downstream of the orifice are known from free-molecule flow theory. The disadvantages of using such a flow for calibration are that the density is very low to maintain free-molecule flow and the speed ratio is much lower than would occur in the case of a nozzle. However, it does offer many advantages for examining the probe operation which outweigh these disadvantages.

Since the probe is a long cylinder, a rectangular opening was chosen for the orifice geometry. This shape will result in flow properties which are reasonably uniform over the length of the wire and thus would require less correction for flow gradients. While the properties downstream of a circular orifice are well-documented, those for a rectangular orifice could not be found and, thus, are given in this appendix for later use.

We will consider the free-molecule flow from a gas source into a vacuum (Fig. A-1). The orifice has dimensions a and b . Inside the source the velocity distribution function is f_v , the number density is n_v and the temperature is T_v . Let $\bar{\xi}$ be the molecular velocity with \bar{u} the mean velocity. Then the number density at any point B downstream of the orifice is given by the integral

$$n = \int f_v d\bar{\xi} \quad (\text{A-1})$$

where the velocity distribution is given by

$$f_v d\bar{\xi} = \frac{n_v}{(2\pi RT_v)^{3/2}} \exp\left(-\frac{\xi^2}{2RT_v}\right) \xi^2 \sin \varphi d\varphi d\theta d\xi \quad (\text{A-2})$$

The solid angle subtended by dA at B is

$$d\omega = \sin \varphi d\varphi d\theta = \frac{dA \cos \Omega}{d^2} \quad (\text{A-3})$$

where

$$d = \sqrt{x'^2 + y'^2 + z'^2} = \sqrt{x^2 + y^2 + z^2} \quad (\text{A-4})$$

$$\cos \Omega = \frac{x'}{d} \quad (A-5)$$

Then the number is given by

$$n = \frac{n_v}{(2\pi RT_v)^{3/2}} \int_0^\infty \xi^2 \exp\left(-\frac{\xi^2}{2RT_v}\right) d\xi \int_A \frac{\cos \Omega}{d^2} dA \quad (A-6)$$

or, using Eq. (A-2),

$$\frac{n}{n_v} = \frac{1}{4\pi} \int_A \frac{\cos \Omega}{d^2} dA \quad (A-7)$$

The geometric integral in Eq. (A-7) was evaluated by introducing the following coordinate transformation and non-dimensionalization.

$$\begin{aligned} x' &= x \\ y'_1 &= -(y + a/2) & y'_2 &= -(y - a/2) \\ z'_1 &= -(z + b/2) & z'_2 &= -(z - b/2) \end{aligned} \quad (A-8)$$

$$\begin{aligned} X &= \frac{x}{a} & Y &= \frac{y}{a} & Z &= \frac{z}{a} \\ R &= \frac{b}{a} & D &= \frac{d}{a} \\ D^2 &= X^2 + Y^2 + Z^2 \end{aligned} \quad (A-9)$$

The result of the integration is

$$\begin{aligned} \frac{n}{n_v} &= \frac{1}{4\pi} \left[\tan^{-1} \left(\frac{(Y + \frac{1}{2})(Z + R/2)}{X} \left\{ D^2 + Y + RZ + \frac{1}{4}(1 + R^2) \right\}^{-1/2} \right) \right. \\ &- \tan^{-1} \left(\frac{(Y - \frac{1}{2})(Z + R/2)}{X} \left\{ D^2 - Y + RZ + \frac{1}{4}(1 + R^2) \right\}^{-1/2} \right) \\ &- \tan^{-1} \left(\frac{(Y + \frac{1}{2})(Z - R/2)}{X} \left\{ D^2 + Y - RZ + \frac{1}{4}(1 + R^2) \right\}^{-1/2} \right) \\ &\left. + \tan^{-1} \left(\frac{(Y - \frac{1}{2})(Z - R/2)}{X} \left\{ D^2 - Y - RZ + \frac{1}{4}(1 + R^2) \right\}^{-1/2} \right) \right] \end{aligned} \quad (A-10)$$

The x-component of the velocity at any point B can be calculated from the integral

$$nu_x = \int \xi_x f_v \bar{d\xi} \quad \xi_x = \xi \cos \Omega \quad (A-11)$$

Using Eq. (A-2) this becomes

$$nu_x = \frac{n_v}{(2\pi RT_v)^{3/2}} \int_0^\infty \xi^3 \exp\left(-\frac{\xi^2}{2RT_v}\right) d\xi \int_A \frac{\cos^2 \Omega}{d^2} dA \quad (\text{A-12})$$

$$\frac{u_x}{\sqrt{2RT_v}} \left(\frac{n}{n_v}\right) = \frac{1}{2\pi^{3/2}} \int_A \frac{\cos^2 \Omega}{d^2} dA \quad (\text{A-13})$$

Notice that the velocity relation has been non-dimensionalized in terms of the speed ratio

$$S = \frac{u_x}{\sqrt{2RT_v}}$$

The evaluation of the geometric integral gives the following relation for the velocity (or speed ratio) at any point B .

$$\begin{aligned} 4\pi^{3/2} \left(\frac{n}{n_v}\right) \frac{u_x}{\sqrt{2RT_v}} = & \\ & - \frac{X^2}{(Y - \frac{1}{2})\sqrt{X^2 + Y^2 - Y + \frac{1}{4}}} \left[\tan^{-1} \left(\frac{Z - R/2}{\sqrt{X^2 + Y^2 - Y + \frac{1}{4}}} \right) \right. \\ & \quad \left. - \tan^{-1} \left(\frac{Z + R/2}{\sqrt{X^2 + Y^2 - Y + \frac{1}{4}}} \right) \right] \\ & + \frac{X^2}{(Y + \frac{1}{2})\sqrt{X^2 + Y^2 + Y + \frac{1}{4}}} \left[\tan^{-1} \left(\frac{Z - R/2}{\sqrt{X^2 + Y^2 + Y + \frac{1}{4}}} \right) \right. \\ & \quad \left. - \tan^{-1} \left(\frac{Z + R/2}{\sqrt{X^2 + Y^2 + Y + \frac{1}{4}}} \right) \right] \\ & + X \left(\frac{1}{Y + \frac{1}{2}} - \frac{1}{Y - \frac{1}{2}} \right) \left[\tan^{-1} \left(\frac{Z + R/2}{X} \right) - \tan^{-1} \left(\frac{Z - R/2}{X} \right) \right] \\ & - \frac{(Z - R/2)}{\sqrt{X^2 + Z^2 - RZ + R^2/4}} \left[\tan^{-1} \left(\frac{Y + \frac{1}{2}}{\sqrt{X^2 + Z^2 - RZ + R^2/4}} \right) \right. \\ & \quad \left. - \tan^{-1} \left(\frac{Y - \frac{1}{2}}{\sqrt{X^2 + Z^2 - RZ + R^2/4}} \right) \right] \end{aligned} \quad (\text{A-14})$$

$$\begin{aligned}
 & + \frac{(Z + R/2)}{\sqrt{X^2 + Z^2 + RZ + R^2/4}} \left[\tan^{-1} \left(\frac{Y + \frac{1}{2}}{\sqrt{X^2 + Z^2 + RZ + R^2/4}} \right) \right. \\
 & \quad \left. - \tan^{-1} \left(\frac{Y - \frac{1}{2}}{\sqrt{X^2 + Z^2 + RZ + R^2/4}} \right) \right] \\
 & + X \left(\frac{1}{Y + \frac{1}{2}} - \frac{1}{Y - \frac{1}{2}} \right) \left[\sin^{-1} \left(\frac{X}{\sqrt{X^2 + Z^2 - RZ + R^2/4}} \right) \right. \\
 & \quad \left. - \sin^{-1} \left(\frac{X}{\sqrt{X^2 + Z^2 + RZ + R^2/4}} \right) \right] \\
 & - \sqrt{1 + \left(\frac{X}{Y - \frac{1}{2}} \right)^2} \left[\sin^{-1} \left(\sqrt{\frac{X^2 + Y^2 - Y + \frac{1}{4}}{D^2 - Y - RZ + \frac{1}{4}(1 + R^2)}} \right) \right. \\
 & \quad \left. - \sin^{-1} \left(\sqrt{\frac{X^2 + Y^2 - Y + \frac{1}{4}}{D^2 - Y + RZ + \frac{1}{4}(1 + R^2)}} \right) \right] \\
 & + \sqrt{1 + \left(\frac{X}{Y + \frac{1}{2}} \right)^2} \left[\sin^{-1} \left(\sqrt{\frac{X^2 + Y^2 + Y + \frac{1}{4}}{D^2 + Y - RZ + \frac{1}{4}(1 + R^2)}} \right) \right. \\
 & \quad \left. - \sin^{-1} \left(\sqrt{\frac{X^2 + Y^2 + Y + \frac{1}{4}}{D^2 + Y + RZ + \frac{1}{4}(1 + R^2)}} \right) \right]
 \end{aligned}$$

The temperature at point *B* can be determined from the following integral

$$nRT = \frac{1}{3} \int \left(\bar{\xi} - \bar{u} \right)^2 f_v d\bar{\xi} = \frac{1}{3} \left[\int \xi^2 f_v d\xi - n u_z^2 \right] \quad (A-15)$$

The first term can be evaluated as follows

$$\begin{aligned}
 \int \xi^2 f_v d\xi &= \frac{n_v}{(2\pi RT_v)^{3/2}} \int_0^\infty \xi^4 \exp \left(-\frac{\xi^2}{2RT_v} \right) d\xi \int_A \frac{\cos \Omega}{d^2} dA \\
 &= \frac{3}{4\pi} n_v RT_v \int_A \frac{\cos \Omega}{d^2} dA = 3nRT_v
 \end{aligned}$$

when use is made of Eq. (A-7). Then the temperature distribution can be written as

$$nRT = nRT_v - \frac{1}{3} n u_z^2$$

$$\frac{T}{T_v} = 1 - \frac{1}{3} \frac{u_x^2}{RT_v} \quad (\text{A-16})$$

$$\frac{T}{T_v} = 1 - \frac{2}{3} s^2 \quad (\text{A-17})$$

The number density profiles in the plane $Y = 0$ are shown in Fig. A-2 for four distances downstream of the orifice plane. The number density has been normalized by its value upstream of the orifice. The profiles are reasonably flat over the length of the wire (to $Z = 5.2$). Fig. A-3 shows the corresponding speed ratio profiles at the same locations. Notice that the speed ratio is always less than 1.0; at large X it would approach a limit of $2/\sqrt{\pi}$ on the centerline. Therefore, the speed ratio can never approach the high values observed in the nozzle and plume and this is one of the major disadvantages of using this flow for calibration purposes. The advantages are that the density is well known at any location from the theory so that the probe operation can be verified without a separate density measurement.

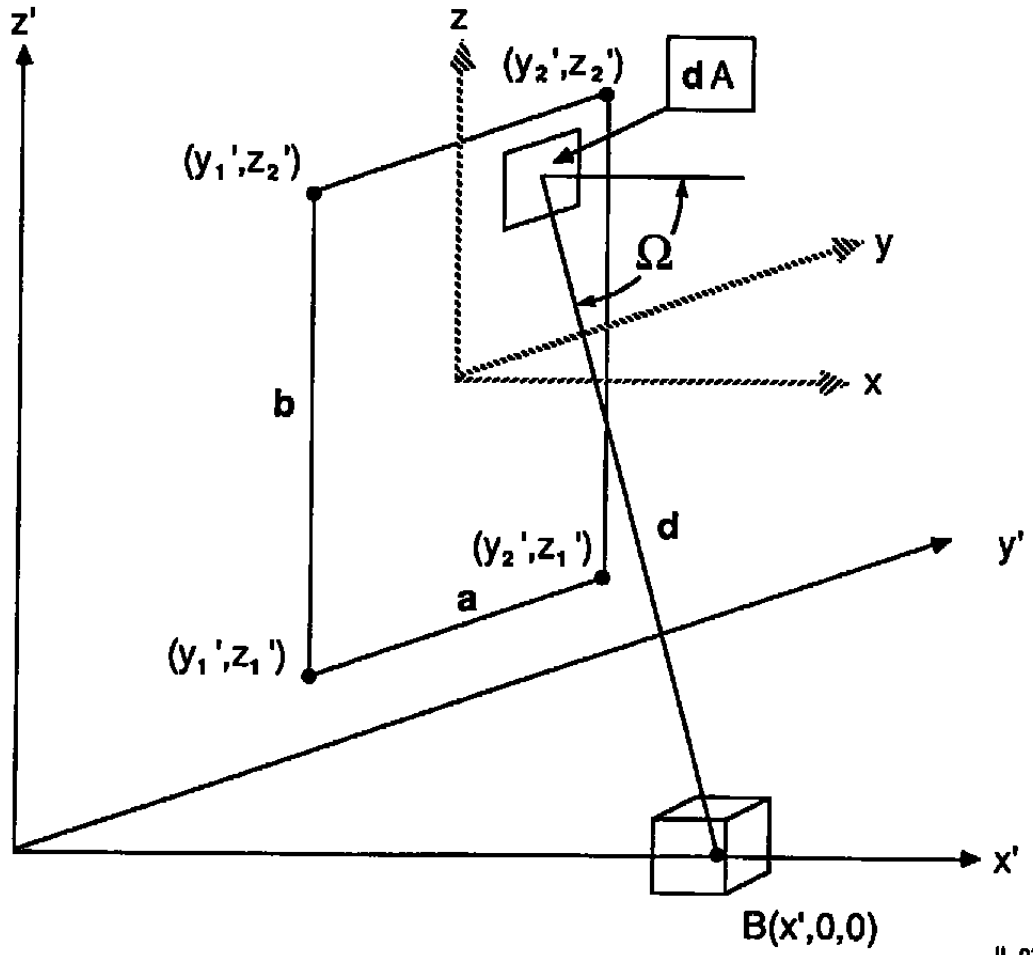


Figure A-1. Geometry used for calculations of flow through rectangular orifice.

IL-0393

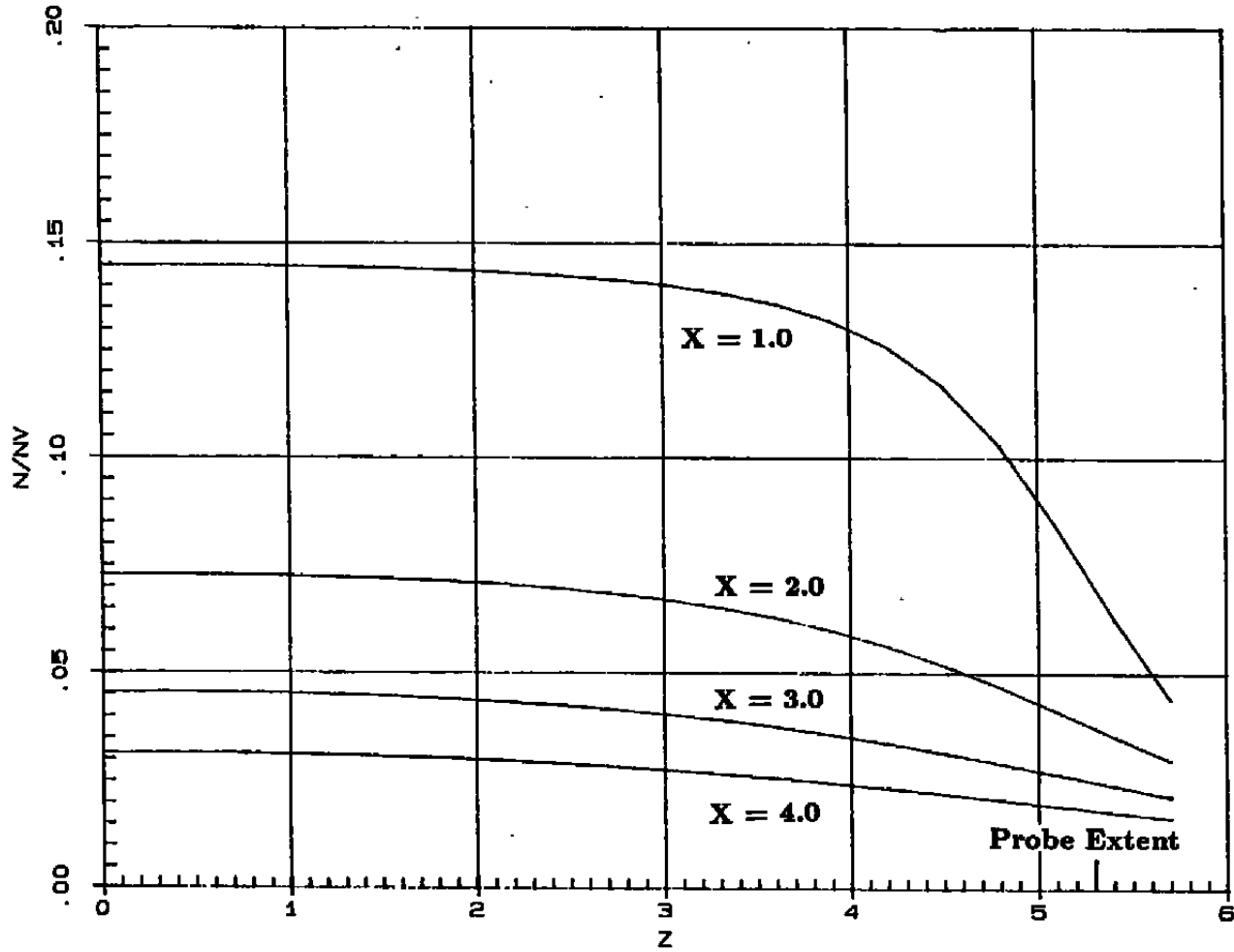


Figure A-2. Number Density Profiles Downstream of a Rectangular Orifice for Free - Molecule Flow.
 $R = 10.5$

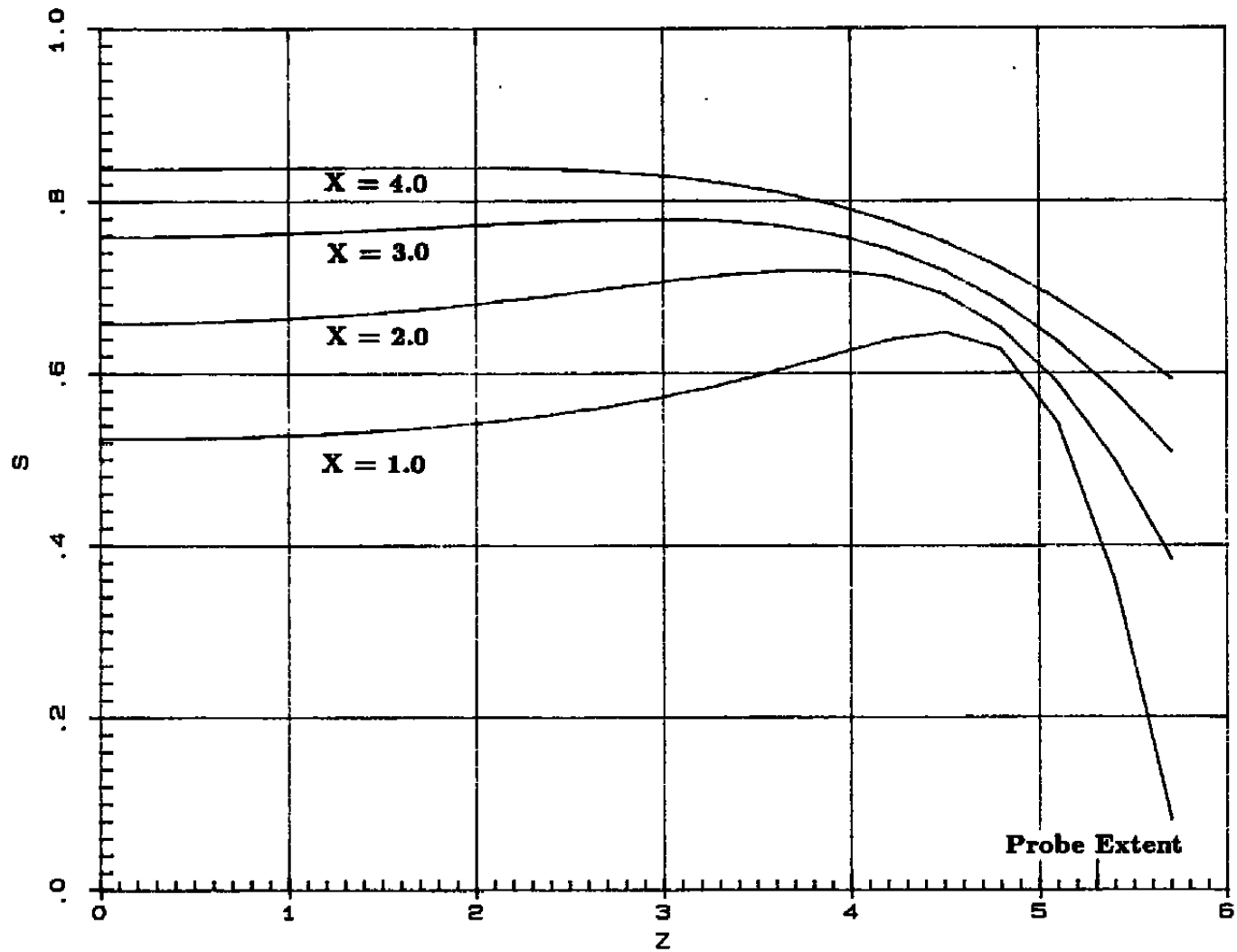


Figure A-3. Speed Ratio Profiles Downstream of a Rectangular Orifice
for Free - Molecule Flow.
 $R = 10.5$

NOMENCLATURE

A	Function defined in Eq. (33)
A_e	Exit area of nozzle
A_s	Surface Area of wire, πDL
A_t	Throat area of nozzle
B	Function defined in Eq. (34)
C	Function defined in Eq. (39), $A + \alpha_r B$
C_F	Isentropic thrust coefficient
C_{F_m}	Measured thrust coefficient
c_v	Specific heat at constant volume of gas at static temperature
c_p	Specific heat at constant pressure of gas at static temperature
\bar{c}	Average molecular speed, $\sqrt{\frac{8}{\pi} \tilde{R}T}$
D	Wire diameter
F	Function defined in Eq. (13)
$f(s)$	Function defined in Eq. (5)
$g(s)$	Function defined in Eq. (6)
H	Enthalpy of gas at static temperature
h_c	Convective heat transfer coefficient from wire, $Q_c/[A_s(T_w - T_{sw})]$
I	Wire current
$I_\nu(z)$	Modified Bessel function of first kind and order ν
j	Number of $kT/2$ units of internal energy carried by molecule
K	Thermal conductivity of gas at static temperature
$K(s)$	Function defined in Eq. (10)
Kn	Knudsen number, λ/D
K_w	Thermal conductivity of wire material
k	Boltzmann constant
L	Length of wire
M	Free stream Mach number
m	Mass of gas molecule
m_∞	Function defined in Eq. (44)
n	Gas number density
Nu	Nusselt number, $h_c D/K$
p	Static gas pressure
p_c	Rocket motor chamber pressure
Pr	Prandtl number of gas $\mu c_p/K$
\dot{Q}	Rate of heat transfer
\tilde{R}	Gas constant of gas
R	Wire resistance

Re	Reynolds number, $\rho v D / \mu$
r	Recovery factor, $\frac{T_{aw} - T}{T_0 - T}$
St	Stanton number, $NuRe/Pr = h_c/\rho c_p V$
s	Speed Ratio, $V/(2\bar{RT})^{1/2}$
T	Temperature
T_s	Temperature at junction of wire and support posts
V	Velocity
V_m	Mean molecular speed, $\sqrt{2\bar{RT}}$
z	Coordinate along wire
X	Function defined in Eq. (41)
Y	Function defined in Eq. (41)
$Z_1, Z_2,$	Functions defined in Eq. (3) and (4)
α	Thermal accommodation coefficient
α_r	Temperature coefficient of resistivity of wire material
ϵ	A_c/A_t
ϵ_w	Emissivity of wire material
γ	Ratio of specific heats, c_p/c_v
λ	Mean free path
μ	Gas viscosity at static temperature
ρ	Gas density, nm
σ	Stefan-Boltzmann constant
θ	$T_w - T_{aw}$

SUBSCRIPTS

a	Reference
aw	Adiabatic wall (equilibrium)
c	Convection
i	Impact
j	Joule heating
k	Conduction
o	Stagnation
r	Rotational
t	Thermistor heating
tr	Translational
w	Wire
w_∞	Infinitely long wire
∞	Solid Walls surrounding probe